Conditions for maximum operating efficiency of a multi-junction solar cell and a proton exchange membrane electrolyser system for hydrogen production

Warren Gies

A thesis submitted in partial fulfillment of the requirements for the
Master of Science degree in Physics

Department of Physics
Faculty of Science
University of Ottawa

Abstract

Hydrogen is a valuable and versatile energy currency; it may be produced by harvesting solar energy and later used as a fuel to generate electricity any time of the day. This energy transaction of solar energy to hydrogen is evaluated in this work by employing a one-to-one multi-junction solar cell to proton exchange membrane combined system in a laboratory setting. Both components of the system were commercially available. The energy conversion efficiency of each isolated system was first evaluated to determine the ideal operation conditions of each respective system. For input currents in the range of 60 mA to 440 mA, the proton exchange membrane converted electrical energy to chemical potential energy with an efficiency greater than 90%. The multi-junction solar cell reached efficiencies of up to 33% while under a solar concentration of 30 Suns. The current and voltage characteristics, which resulted in the optimal operation of the isolated systems did not align and therefore, both systems were not operating at their ideal operation conditions when in the combined system. The overall energy conversion efficiency of the system was measured to be at most 19.1% under 25 Suns, an efficiency higher than systems employing traditional silicon solar cells. It was theorized that if the two system were operating under ideal conditions, the overall energy conversion efficiency would be 30.3% between 10 and 15 Suns. Methods to align the ideal operation conditions of the two systems are presented.

Statement of Originality

The results presented in this work are based on measurements and analysis performed by Warren Gies for the partial fulfillment of the requirements for his Master of Science thesis research project under the supervision of Dr. Karin Hinzer. All results are original. Supporting information from other sources are cited.

This project was developed through the NSERC CREATE TOP-SET project (Training in Optoelectronics for Power: From Science and Engineering to Technology). The goal of this thesis was to contribute to the scientific community focused on the development of sustainable renewable energy systems.

Acknowledgements

I would like to thank Dr. Karin Hinzer for giving me the opportunity to pursue this degree and develop my research skills. I thank her for her ongoing guidance and patience. I appreciate the knowledge and advice she shared with me. I would also like to thank Dr. Chris Valdiva, Dr. John Cook, Dr. Javad Fattahi, Dr. Matthew Wilkins and Dr. Ross Cheriton for their sharing their technical knowledge and support in the laboratories. I would also like to thank them for their valuable feedback during the progression of my research. I would like to thank my fellow SUNLAB graduate students including Meaghan Beattie, Gavin Forcade, Kayden Kaller, Robert Pollak, Erin Tonita, and Matheus Fonseca. Each member shared their specific knowledge to help me strengthen my research project for which I am very thankful. I would finally like to thank my family for providing me with needed ancillary support.

Contents

1 Introduction ..... - 1 -

1.1 Purpose ..... - 1 -

1.2 Scope ..... - 2 -

1.3 Overview ..... - 2 -

2 Background and Theory ..... - 4 -

2.1 PEM electrolyser ..... - 4 -

2.1.1 Hydrogen as an energy carrier ..... - 5 -

2.1.2 Thermodynamics of electrolysis ..... - 5 -

2.1.3 PEM electrolyser energy conversion efficiency ..... - 8 -

2.2 MJSC ..... - 10 -

2.2.1 MJSC efficiency ..... - 12 -

2.2.2 Solar energy spectra ..... - 15 -

2.3 The combined electrolyser PV system ..... - 17 -

2.3.1 Combined system configuration ..... - 17 -

2.3.2 Solar to hydrogen efficiency ..... - 18 -

2.3.3 System matching ..... - 19 -

3 Experimental Methods ..... - 21 -

3.1 Introduction ..... - 21 -

3.2 Equipment background ..... - 21 -

3.2.1 Solar simulator ..... - 21 -

3.2.2 Source meters ..... - 23 -

3.2.3 Temperature controller system ..... - 24 -

3.3 Electrolyser measurements ..... - 26 -

3.3.1 PEM electrolyser energy conversion efficiency ..... - 26 -
3.4 Solar measurements ..... - 28 -
3.4.1 General conditions ..... - 28 -
3.4.2 Determination of one Sun short circuit current for the test MJSC ..... - 29 -
3.4.3 Multi-junction solar cell energy conversion efficiency measurements ..... - 31 -
3.5 Combined system ..... - 32 -
3.5.1 STH energy conversion efficiency ..... - 32 -
4 Results and Analysis ..... - 34 -
4.1 PEM electrolyser ..... - 34 -
4.1.1 Theoretical production of hydrogen gas ..... - 34 -
4.1.2 Voltage-time measurements ..... - 37 -
4.1.3 Energy conversion efficiency of the PEM electrolyser ..... - 38 -
4.1.4 Experimental set up evaluation ..... - 41 -
4.1.5 Polarization curve of the PEM electrolyser ..... - 42 -
4.1.6 Purity of produced $\boldsymbol{H2}(\boldsymbol{g})$ and $\boldsymbol{O2}(\boldsymbol{g})$ ..... - 45 -
4.2 MJSC ..... - 46 -
4.2.1 Solar simulator calibration ..... - 46 -
4.2.2 Characteristics of the MJSC ..... - 47 -
4.2.3 Efficiency of the MJSC ..... - 52 -
4.3 Combined system ..... - 55 -
4.3.1 Efficiency of the PEM electrolyser with power supplied by the MJSC ..... - 55 -
4.3.2 Efficiency of the MJSC when powering the PEM electrolyser ..... - 57 -
4.3.3 Overall Energy Conversion Efficiency ..... - 59 -
5 Conclusions ..... - 62 -

5.1 Summary ..... - 62 -
5.2 Future work ..... - 62 -
6 Appendices ..... - 65 -
6.1 Uncertainty of measurements ..... - 65 -
6.2 PEM electrolyser results summary ..... - 66 -
6.3 References ..... - 68 -

List of abbreviations

AM – Air mass

ASTM – American society for testing and materials

DC – Direct current

HHV – Higher heating value

I-U – Current-voltage

LHV – Lower heating value

MJSC – Multi-junction solar cell

NREL – National renewable energy laboratory

PEM - Proton exchange membrane

PV – Photovoltaics

SATP – Standard atmospheric temperature and pressure

SJSC – Solar junction solar cell

SMU – Source meter unit

STH – Solar to hydrogen

TEC – Thermoelectric cooler

List of Symbols

a, b and c - Steinhart-Hart coefficients

A – Standard error of the mean

B – Uncertainty

$E_{Conduction}$– Conduction band energy (J)

E_{gap} – Band gap energy (J)

E_{Light} – Light energy (J)

$E_{Valence}$ – Valence band energy (J)

F- Faraday's constant

FF – Fill factor

HHV – Higher heating value ($J\ mol^{-1}$)

I – Current (A)

I_{MPP} – Maximum power point current (A)

I_{op} – Operating current (A)

I_{PEM} – Maximum operating current of the PEM electrolyser (A)

I_{SC} – Short circuit current (A)

$I_{sc,1\ sun}$ – Short circuit current of 1 Sun (A)

I_{total} – Total current (A)

MPP – Maximum power point (W)

n – number of modules

n_e - moles of electrons (mol)

n_g – moles of gas molecules (mol)

η_c – Current Efficiency (%)

η_{MJSC} – MJSC efficiency (%)

$\eta_{MJSC,max}$ – Maximum MJSC efficiency (%)

η_{PEM} – PEM Electrolyser Efficiency (%)

η_V – Voltage Efficiency (%)

P – Pressure (Pa)

P_{in} – Input power (W)

P_{out} – Output power (W)

q – Charge (C)

R – Gas constant ($L\ Pa\ K^{-1}\ mol^{-1}$)

R_s – Ratio of PEM electrolysers to MJSCs connected in series

R_p – Ratio of PEM electrolysers to MJSCs connected in parallel

t – Time (s)

T – Temperature (K)

$\Gamma_{1\ Sun}$ – Intensity of 1 Sun ($W\ m^{-2}$)

U_0 – Thermoneutral voltage (V)

U_{MPP} – Maximum power point voltage (V)

U_{OC} – Open circuit voltage (V)

U_{op} – Operating voltage (V)

U_{PEM} – Maximum operating voltage of the PEM electrolyser (V)

U_{total} – Total voltage (V)

V – Volume (L)

$V_{H_2 experimental}$ – Volume of experimental production of hydrogen gas (L)

$V_{H_2 theoretical}$ – Volume of theoretical production of hydrogen gas (L)

V_m – molecular volume ($L\ mol^{-1}$)

X – Solar concentration ratio

z - Number of electrons

Z – Any measured value

List of Figures

Figure 1.1.1: Schematic representation of the process of light energy to stored potential energy from a combined MJSC electrolyser system. .....- 1 -

Figure 2.2.1: Representation of a) the photoexcitation of an electron in a semiconductor when the incident light energy ($ELight$) is greater than the band gap energy ($Egap$ – which is the difference between the energy of the conduction band, $EConduction$, and valence band, $EValence$), the resulting generation of an electron-hole pair and the loss of the excess energy b) the photoexcitation of an electron in a semiconductor and the generation of the electron-hole pair when the incident light energy is equal to the band gap energy, and c) when the incident light energy is less than the band gap energy, the energy is transmitted through the semiconductor. - 11 -

Figure 2.2.2: Highest energy conversion efficiencies of research solar cells determined by certified agencies and laboratories worldwide from 1976 through 2019 for various PV technologies.[20].....- 13 -

Figure 2.2.3: A selection of AM0, AM1.5G, and AM1.5 D solar spectra from ASTM[24][25]. ... - 16 -

Figure 3.2.1: Schematic representation of the light origination and path through the solar simulator, the Sol 3A, to the test MJSC. A power supply (a) is used to ignite the xenon arc lamp (b). All of the irradiance produced from the xenon arc lamp is reflected and directed by the ellipsoid reflector (c) to the primary mirror (d). The primary mirror then redirects the output irradiance towards the partial sun attenuator (e). The partial sun attenuator may be manually opened or closed to alter the output irradiance which then passes though a spectral filter (f) which alters the spectrum of irradiance. The output irradiance continues to a secondary mirror (g) and is redirected to a collimating lens (h) and finally, to the test MJSC. .....- 22 -

Figure 3.2.2: Schematic representation of the TEC system with two p-n junctions connected in series. The materials depicted in green and light grey are n-type and p-type semiconductors, respectively. .....- 25 -

Figure 3.3.1: PEM electrolyser set up used to measure the energy conversion efficiency of the PEM electrolyser. The system consists of a) a Keithley SMU 2420, b) a PEM electrolyser cell, c)

two water reservoir/gas storage tanks, d) two outlet hoses for water and gas expulsion and e) two hose clamps. During measurements, the reference Keithley SMU 2420 would be connected with a computer and the in-house prepared software was used to apply the desired current and concurrently measure the applied current and potential difference across the electrolyser cell over a predetermined period of time. .....- 27 -

Figure 3.3.2: Water reservoir/gas storage tank for the PEM electrolyser, which was used to determine the volume of gas produced over a set period of time. The water reservoir/gas storage tank of the PEM electrolyser is presented a) with no hydrogen b) with 10 mL hydrogen. .....- 28 -

Figure 3.4.1: a) Laboratory set up used to measure the energy conversion efficiency of the MJSC and b) a close up of the MJSC. The system consists of i) a Sol 3A solar simulator, ii) a PV reference cell, iii) a PV reference cell meter, iv) a Keithley TEC 2510-AT SMU, v) a Keithley SMU 2420, vi) a MJSC and vii) a 10 $k\Omega$ NTC Bead Head Thermistor. The MJSC and Thermistor are sitting on the laboratory developed TEC. The cooling fan is placed to the left of the photo. When being used, the reference cell would be placed on the stage where the test cell is in the photo. .....- 30 -

Figure 3.4.2: Previously columnated irradiance is concentrated towards the surface of the test MJSC by use of a Fresnel lens. .....- 31 -

Figure 3.5.1: The instrument and equipment configuration of the combined MJSC and PEM electrolyser system used to measure the STH energy conversion efficiency. The necessary equipment and instrumentation to measure the efficiency consisted of a) a Sol 3A solar simulator, b) a Fresnel lens, c) a 1600 Watt arc lamp power supply, d) a MJSC on the

temperature control system, e) a Keithley TEC 2510-AT SMU, f) a Keithley SMU 2420, and g) an Electrolyser 5 electrolyser system. ..... - 33 -

Figure 4.1.1: Time required to produce 27.5 mL of hydrogen gas with the PEM electrolyser assuming a 100% current efficiency. ..... - 36 -

Figure 4.1.2: Measured voltage across the PEM electrolyser while under an applied current at 7 of the 60 input currents ..... - 38 -

Figure 4.1.3: Faraday, voltage, and overall energy conversion efficiency of the PEM electrolyser- 41 -

Figure 4.1.4: Polarization curve of the PEM electrolyser. The area in red identifies the area that results in an energy conversion efficiency of 90% or more. ..... - 44 -

Figure 4.2.1: a) I-U curve and b) power-voltage curve of the test MJSC at SATP under various levels of illuminations. In chart a), the X's for each trial's data indicates the location of the MPP. ..... - 49 -

Figure 4.2.2: Fill factor of the test MJSC at SATP under varying solar concentrations. ..... - 51 -

Figure 4.2.3: Efficiency of the test MJSC at SATP under varying solar concentrations. ..... - 53 -

Figure 4.3.1: Efficiency of the PEM electrolyser when powdered by the MJSC ..... - 56 -

Figure 4.3.2: I-U curve of the PEM electrolyser and the test MJSC under various levels of illuminations at SATP. The X's indicate the location of the combined system's operating power point and the +'s indicate the MPP of the MJSC. ..... - 58 -

Figure 4.3.3: Efficiency of the MJSC at different solar concentrations at the MPP of the MJSC, and efficiency of the cell at the voltage produced by the electrolyser, the operating power point.. - 59 -

Figure 4.3.4: Solar to hydrogen efficiency of the combined PEM electrolyser and MJSC system. - 60 -

List of Tables

Table 4.2.1: Characteristics of the MJSC summary .....- 51 -

Table 4.3.1: Summary of PEM electrolyser efficiency when powered by the MJSC .....- 57 -

Table 6.1.1: Measurement accuracy of instruments .....- 65 -

Table 6.2.1: Summary of PEM Results .....- 66 -

1 Introduction

1.1 Purpose

The global progression towards renewable energy resources is ever increasing. Considerations of not only clean energy production, but also efficient methods of energy storage are key aspects towards the development of reliable, functional, and robust renewable energy systems [1]. This is particularly true for solar photovoltaic (PV) energy conversion systems, which harvest the naturally abundant energy from the sun to produce electrical energy. Without a method to efficiently store solar energy, these systems are limited for use in sunny conditions. This problem is compounded by the mismatch between energy demands and solar intensity; energy demands in Ontario are highest at 9 A.M. and 6 P.M. in the winter, and 2 P.M. in the summer [2] while solar intensity is at its peak at noon. Isolated solar energy systems would be impractical for widespread use if there was not an efficient method to store the produced energy when they are not directly connected to the grid. The traditional method of energy storage was the use of batteries. Though batteries provide a method to store energy from solar energy harvesting systems, they have a very limited life time and are expensive to both purchase and safely dispose of at the end of their life cycle.

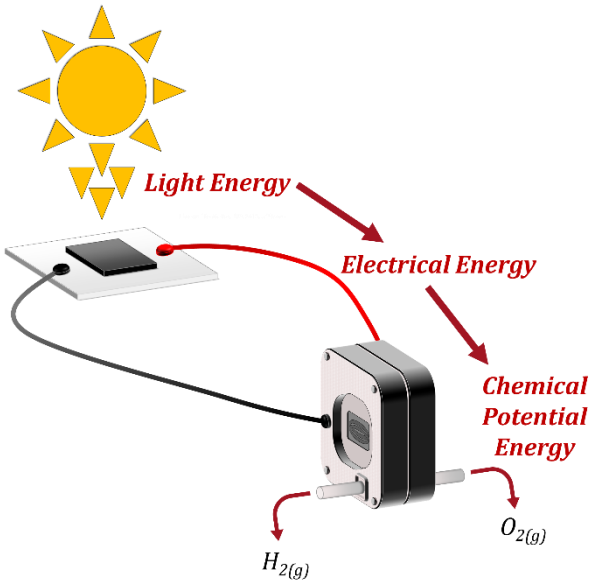

Figure 1.1.1: Schematic representation of the process of light energy to stored potential energy from a combined MJSC electrolyser system.

Solar cell and electrolyser systems provide a solution to this limitation by both harvesting and storing the energy from the sun. In this process, the primary energy source, solar light energy, is transformed into electrical energy by a solar cell. The electrolyser converts the electrical energy into stored chemical potential energy in the form of hydrogen gas. A representative illustration of this process is displayed in Figure 1.1.1. Hydrogen gas is a secondary energy source and may be

used as fuel to generate electrical energy, regardless of the presence of the sun. Hydrogen is considered a key component of the future of renewable energy systems[3].

For renewable energy systems to be commercially viable, they must be comparable in price or provide a significant benefit over their non-renewable counterparts. As such, systems are routinely being optimized to maximize efficiency and reduce the cost per watt of point of use electricity. It is important to have reliable methods to measure the efficiency to effectively evaluate and compare systems and system modifications.

1.2 Scope

The scope of this thesis was to determine the practical solar-to-hydrogen (STH) energy conversion efficiency of a single high-efficiency multi-junction solar cell (MJSC) and a single proton exchange membrane (PEM) electrolyser system in a laboratory setting. This one-to-one model neglects operating efficiency, but provides valuable information about the isolated and single units information, which is essential for modeling. A secondary purpose of this series of experiments was to contribute to the scientific community by studying the finer details of the experimental set up to perform quality measurements.

1.3 Overview

The second chapter details the relevant background and theory of electrolysis, photovoltaics, and the combined system. General information is presented on electrolysis and the systems used to accomplish this process. It also includes a detailed outline on hydrogen including its production through electrolysis, and methods of measuring its production efficiency. Furthermore, the process for capturing solar energy, including the efficiency of these devices is discussed, as is the overall STH process.

The specifics of the experiments and experimental methods performed in this work are outlined in Chapter 3. Details on the experimental set up, which was used to measure the STH efficiency of a combined MJSC electrolyser system, as well as each system in isolation, are provided. Experimental set up details include the equipment used and the procedures followed to obtain the measurements. Information on the reagents, equipment brands, and suppliers is also included.

The purpose of this chapter is to provide all of the necessary information to allow this work to be reproduced, or built upon by other researchers.

Chapter 4 of this work presents the results obtained through conducting the experiments detailed in Chapter 3. The efficiency of the electrolyser is presented as are its characteristic current-voltage (*I-U*) properties. The conditions, which result in the maximum efficiency of the PEM electrolyser, are presented. The analysis regarding the purity of the gases produced by the PEM electrolyser is presented. Following the analysis of the PEM electrolyser, a similar evaluation of the MJSC is presented. The *I-U* characteristics of the MJSC are presented and used to determine the conditions, which result in the maximum operation efficiency. The results of the combined system are then presented. The results of the combined efficiency include the actually obtained STH efficiency, as well as a theorized maximum.

Chapter 5 presents a summary of the important findings of this work. There are interesting aspects of this research topic that were not explored under the scope of this work. Ideas for the future development of this project are outlined in Chapter 6.

2 Background and Theory

2.1 PEM electrolyser

The electrolyser is a device, which uses electrical energy to split liquid water into its elements, hydrogen and oxygen, in their gaseous form. Presently there are three principal categories of electrolysers, which are awarded significant attention in current literatures: alkaline electrolysers, PEM electrolysers and solid oxide and proton ceramic electrolysers. Alkaline electrolysers are composed of an anode and cathode containing a precious metal catalyst, which are submerged in an alkaline electrolyte, typically potassium hydroxide. Oxygen is produced at the anode and hydrogen ions diffuse to the cathode to react to form hydrogen gas. The anode and cathode are separated by a semipermeable membrane, which permits the passage of water and small positively charged ions, but is theoretically impermeable to hydrogen and oxygen gas. Alkaline electrolysers are commonly criticized for the significant amount of parasitic leakage of oxygen and hydrogen through the membrane, as well as their use of corrosive chemicals. Furthermore, alkaline electrolysers have a very limited range of operation conditions due to the aqueous electrolyte. PEM electrolysers have a solid electrolyte, typically a polymer functionalized with sulphonic acid groups, which permit the transfer of protons. The electrodes of PEM electrolysers also typically contain precious metal catalysts such as Pt, Ir, or Ru. Compared to alkaline electrolysers, PEM electrolysers produce higher purity gases, can reach higher electrical efficiencies, are smaller, and generally more convenient units. Interestingly, the PEM electrolyser was first used in a commercial setting in the 1950s in the USA to support a NASA space program [4]. The most modern electrolyser is the solid oxide and proton ceramic electrolyser, which is intrinsically different from the other two systems in that oxygen ions are the species to diffuse through the device via the ceramic electrolyte. This opposes the other two systems in which hydrogen ions diffuse through the device to react at the cathode. This electrolyser is only functional at higher temperatures (700°C+) and has not yet reached a significant commercial popularity. For these reasons, the work for this thesis used a PEM

electrolyser. Its characteristics, including the energy conversion efficiency, were studied independently and in combination with a test solar cell in a laboratory setting.

2.1.1 Hydrogen as an energy carrier

Hydrogen is often referred to as an energy currency due to the ease of which it may be produced with energy as an input, and used to produce energy at a later date. In 2012 it was estimated that by year 2050 there will be a hydrogen energy demand of over 42 million metric tons [5], principally at generating stations during off peak periods. Hydrogen is an interesting choice of an energy currency because its production is not geographically limited and it may be used in many consumer items in place of natural gas including internal combustion engines, turbines, ovens, and in new applications like fuel cells [6][7].

2.1.2 Thermodynamics of electrolysis

Broadly, electrolysis is the process by which electricity is passed through a substance to drive a dissociation reaction. The term electrolysis applies to a variety of chemical processes, but this work specifically focuses on the electrolysis of water by an electrolyser.

The dissociation reaction of liquid water into oxygen and hydrogen gas is nonspontaneous and requires the input of electricity to drive the reaction. Under standard atmospheric temperature

and pressure (SATP) (298 K, 1 atm), the dissociation reaction is defined by the following equation:

$$H_2O_{(l)} \rightarrow H_{2(g)} + \frac{1}{2}O_{2(g)} \quad (1)$$

where $H_2O_{(l)}$, $H_{2(g)}$, and $O_{2(g)}$ represent liquid water, hydrogen gas and oxygen gas respectively. Equation (1) is the sum of two half reactions, which are defined by the following equations:

$$H_2O_{(l)} \rightarrow \frac{1}{2}O_{2(g)} + 2H^+_{(aq)} + 2e^- \quad (2)$$

$$2H^+_{(aq)} + 2e^- \rightarrow H_{2(g)} \quad (3)$$

where equation (2) takes place at the anode and equation (3) takes place at the cathode.

As this reaction is nonspontaneous, electrical and thermal energy are both reactants as per the following equation:

$$H_2O_{(l)} + 237.2\ kJ\ mol^{-1}\ (electricity) + 48.6\ kJ\ mol^{-1}\ (heat) \rightarrow H_{2(g)} + \frac{1}{2}O_{2(g)} \quad (4)$$

The source of thermal energy for this reaction is produced internally as a result of the internal resistance of the electron and proton currents [8]. The thermoneutral voltage is the minimum voltage required for the reaction to occur, assuming all of the heat generated in the reaction is used to drive the reaction and is not lost. The thermoneutral voltage may be determined by considering the total energy required for the reaction, also referred to as the higher heating value (HHV), per the number of electrons necessary to create one molecule of hydrogen and Faraday's

constant, which represents the magnitude of electric charge per mole of electrons. The thermoneutral voltage, U_0, is calculated by the following equation:

$$U_0 = \frac{HHV}{zF} = \frac{285.84\ kJ\ mol^{-1}}{2\ (96485\ C\ mol^{-1})} = 1.481\ V \tag{5}$$

where HHV is in kilojoules per mole, z is the number of electrons transferred per ion, and F is Faraday's constant in coulombs per mole. The above equation can be rearranged for *HHV*:

$$HHV = U_0 zF \tag{6}$$

The *HHV* takes into account the enthalpy of evaporation and the latent heat of vaporization of liquid water during the formation of oxygen and hydrogen gas from liquid water.

Under high temperature electrolysis, the lower heating value (*LHV*) is used instead of the *HHV* to determine the thermodynamic voltage of the reaction. The LHV accounts for the transition of hydrogen gas and oxygen gas back into liquid water, which does not occur in this series of experiments; oxygen and hydrogen are both collected in their gaseous form at SATP [9]. When the LHV is used, the thermodynamic voltage is 1.25 V.

Another important form of potential energy to report is the free energy voltage, which has a value of 1.23 V. The free energy voltage value only considers the electrical energy required for electrolysis ($237.2\ kJ\ mol^{-1}$). This potential is often used because the thermal energy is obtained from heat generated by molecular interactions within the cell itself. In practice, electrolysis of water is not possible at or below this potential. Water electrolysis occurs at cell potentials between the free energy voltage and the thermoneutral voltage; however, a constant system temperature cannot be maintained [10]. Since the scope of this thesis considers the

electrolyser under SATP, the energy conversion efficiency for the PEM electrolyser considered the HHV as the minimum voltage required for the dissociation reaction to occur.

2.1.3 PEM electrolyser energy conversion efficiency

The energy conversion efficiency for electrolysis is the product of two efficiencies, the voltage efficiency (η_v) and the current efficiency (η_c):

$$\eta_{PEM} = \eta_V \eta_C \tag{7}$$

Since the thermoneutral voltage is the minimum voltage required for electrolysis, operating at any voltage above this point contributes to a loss in energy conversion efficiency. The voltage efficiency for electrolysis is displayed in the following equation:

$$\eta_v = \frac{U_0}{U_{op}} \times 100\% \tag{8}$$

where U_{op} is the operating voltage in volts during electrolysis. In contrast, the current efficiency is not simply a ratio and considers many experimental factors.

To determine the current efficiency, some experimental parameters must first be presented. The scope of this thesis focused on constant as opposed to fluctuating current input during electrolysis. For constant current electrolysis, charge can be represented as:

$$q = It \tag{9}$$

where q, I and t represent charge in coulombs, constant current in amperes, and time in seconds, respectively. Furthermore, Faraday's second law of electrolysis applies this assumption of

constant current and provides a method for calculating the number of moles of electrons. Faraday's second law of electrolysis states:

$$n_e = \frac{It}{zF} \tag{10}$$

where n_e is the number of moles of electrons. Since the PEM electrolysis experiments conducted for the thesis were performed using a constant input current at SATP, the above equations can be utilized for determining the current efficiency, also known as the electrical efficiency or the Faraday efficiency. Additionally, since the molecular mass of hydrogen is a well-established value and hydrogen gas is considered an ideal gas, the ideal gas law can be employed to obtain the molar volume of hydrogen. The ideal gas law states:

$$PV = n_g RT \tag{11}$$

where P, V, R, n_g and T represent the pressure in atmospheres, the volume in liters, the gas constant in liter atmospheres per mole kelvins, the number of moles of the ideal gas, and the temperature in kelvins, respectively. Using the assumptions stated above along with equation (11), the molar volume of hydrogen at SATP can be defined as follows:

$$V_m = \frac{V}{n} = \frac{RT}{P} \tag{12}$$

Furthermore, using Faraday's second law of electrolysis from equation (10) and the molecular volume of hydrogen from equation (12), the theoretical hydrogen production under constant input current electrolysis can be calculated as follows:

$$V_{H_2 theoretical} = \frac{I_{op} t V_m}{zF} \tag{13}$$

where I_{op} is the input current or operating current in amperes and t is the time of the experiment in seconds. Using the input current and duration of the experiment, a theoretical volume of hydrogen production can be calculated and compared with the experimental production of hydrogen to evaluate the current efficiency of the system. Additionally, the equation above can be rearranged to solve for time in order to determine how long an experiment should be carried

out to reach an approximate level of hydrogen production for systems with limited hydrogen storage capacity. The current efficiency is defined by the following equation:

$$\eta_C = \frac{V_{H_2 experimental}}{V_{H_2 theoretical}} \times 100\% \tag{14}$$

Since the energy conversion efficiency for the PEM electrolyser is a product of the voltage and current efficiencies, the energy conversion efficiency is defined and simplified from equations (6) and (13) in the following equation:

$$\eta_{PEM} = \frac{U_0}{U_{op}} \frac{V_{H_2 experimental}}{V_{H_2 theoretical}} \times 100\% = \frac{HHV\ V_{H_2 experimental}}{U_{op} \mathrm{I_{op}} t V_m} \times 100\% \tag{15}$$

Equation (15) provides a method to measure the energy conversion efficiency of the electrolyser system to convert electrical energy into chemical potential energy in the form of hydrogen gas. High efficiency PEM electrolysers can reach energy conversion efficiencies of 90% or higher when the HHV is used to calculate efficiency [11][12].

2.2 MJSC

All PV devices rely on the principle that light energy has the ability to excite electrons from bound states to higher energy levels where they are able to move more freely. This phenomenon was first reported by Edmund Bequerel in 1839 in a case where a current was produced as a result of the illumination of a silver coated platinum electrode in an electrolytic solution [13]. It was in 1876 that the first solid state PV device was made using selenium and heated platinum contacts. It was not until the 1950s when PV devices were of similar design to today's modern systems when silicon p-n junction solar cells became popular.

MJSCs are PV devices, which consist of layers of individual semiconductor p-type in which the majority of charge carriers are holes (lack of electrons), and semiconductor n-type in which the majority of charge carriers are electrons, which are connected in series. Incident light excites electrons of a semiconductor from the lower energy valence band into the higher energy

conduction band and generates an electron-hole pair and drives a current. The energy level difference between the valence and conduction bands is the band gap, which varies depending on the type and properties of the semiconductor. As incident light contains a spectrum of energies, some wavelengths are insufficient to generate an electron-hole pair and are transmitted through the solar cell, and others are too great such that the excess energy is lost as heat. This phenomenon is known as thermalization losses and is represented in Figure 2.2.1. MJSCs minimize thermalization losses by having multiple bandgaps so that a greater portion of the solar spectrum is closer to a bandgap energy, resulting in less wasted energy. Referring to the panels in Figure 2.2.1, compared to single junction solar cells (SJSC), in MJSCs there are more instances of panel b) where the incident light is equal, or very close, to the band gap energy and there are fewer instances of panels a) and c) where energy is lost. The semiconductor sub-cells are layered in the MJSC so that the top cell has the highest energy band gap and the bottom cell has the lowest energy band gap. This orientation makes it so that the portion of the solar spectrum, which is not used to excite electrons passes through the top semiconductor and may excite electrons in the subsequent semiconductors. As the sub-cells of a MJSC are connected in series, the current generated by the MJSC is limited by the sub-cell, which produces the least current.

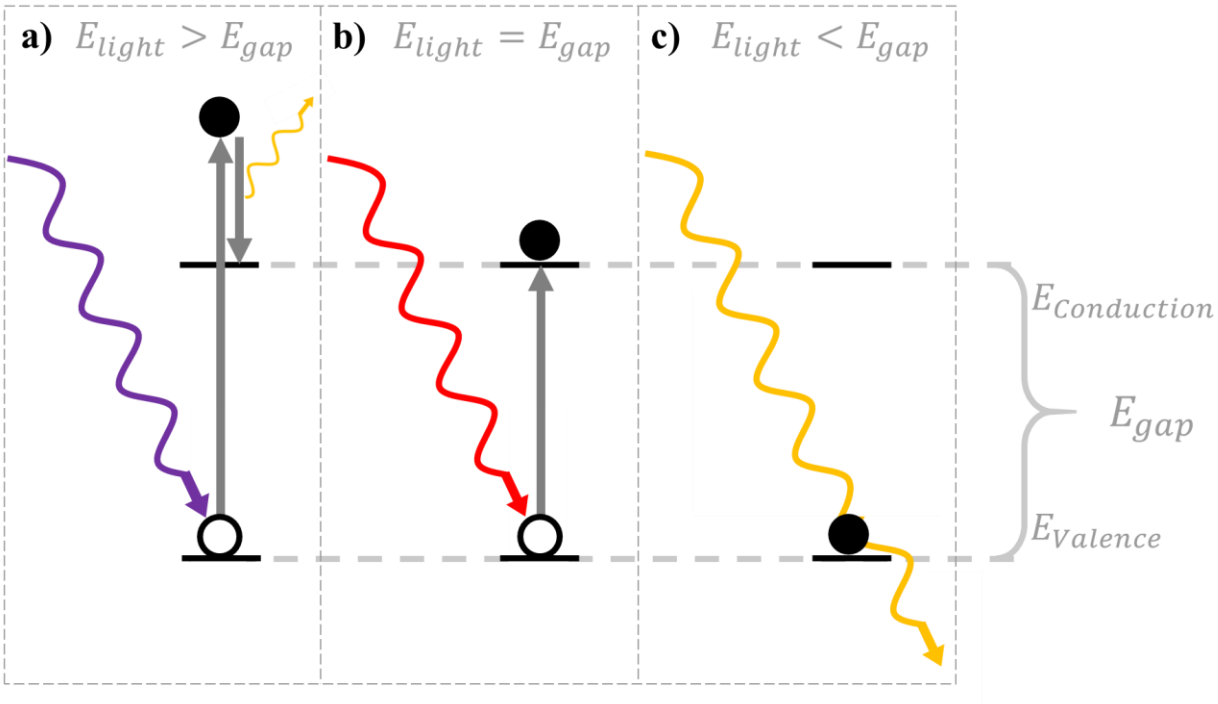

Figure 2.2.1: Representation of a) the photoexcitation of an electron in a semiconductor when the incident light energy (E_{Light}) is greater than the band gap energy (E_{gap} – which is the difference between the energy of the conduction band, $E_{Conduction}$, and

valence band, $E_{Valence}$), the resulting generation of an electron-hole pair and the loss of the excess energy b) the photoexcitation of an electron in a semiconductor and the generation of the electron-hole pair when the incident light energy is equal to the band gap energy, and c) when the incident light energy is less than the band gap energy, the energy is transmitted through the semiconductor and no electron-hole pair is generated.

Within the category of MJSCs, there are many different groups including III-V MJSCs, crystalline silicon (c-Si) MJSCs, and amorphous and nanocrystalline silicon (a-Si/nc-Si) MJSCs [14]. Within these classifications, as a group, III-V MJSCs reach the highest efficiencies and is the type of MJSC used in this work. III-V MJSCs are cells composed of III-V semiconductor compounds and alloys where III and V refer to elemental groups in the periodic table. Group III includes B, Al, Ga, and In and group V includes N, P, As, and Sb. III-V MJSCs typically contain GaInP and/or Ga(In)As [15]. The first III-V MJSC was reported in 1984 and consisted of a two-junction solar cell of GaInP/GaAs. The popularity of this group of semiconductors for applications in MJSCs is due to their high electron mobility, direct band gap, which results in high absorption coefficients, and low exciton binding energy [16]. Typical bandgaps of III-V semiconductors are in the ideal range for PV devices of 0.7 eV to 2 eV, or approximately 600 nm to 1700 nm, which spans across a significant portion of the incident solar spectrum.

2.2.1 MJSC energy conversion efficiency

Compared to the widely commercially available silicon SJSC, which hold over 90% of the commercial market [17], MJSC are much more expensive. In order to justify the higher cost, MJSC must offer a great advantage over their single junction silicon counterparts in energy conversion efficiency. Though the performance of silicon SJSC has greatly improved since their commercial induction, their efficiency has peaked just over 25% [18], with the record being 26.7% in 2017 [19]. As this record is very close to the detailed balance limit, also known as the Shockley-Queisser limit, theorized in 1961 to be 30% [20], there is not much room for growth. The work of Shockley and Queisser was expanded upon in 1980 to include MJSCs under unconcentrated and concentrated sunlight. It was reported that the detailed balance limit of the performance of a MJSC with an infinite number of junctions was 68% under unconcentrated sunlight, which raised to 86% with concentration. From this, it is evident that significantly higher efficiencies may be reached with MJSCs and that concentration further increases achievable efficiencies. Of course, an infinite MJSC could not be built; they also reported the detailed

balance limit of a three cell MJSC is 63% under concentration. As of 2019, the highest confirmed unconcentrated terrestrial MJSC efficiency reached is 39.2%, which came from the solar cell design reported in the *Solar cell efficiency tables (version 54)* [14]. In the same publication, under concentration of 143 Suns, an efficiency of 47.1% was reached. Both of these record setting efficiencies, along with various other solar cell efficiency records from 1979-2019, are displayed in Figure 2.2.2.

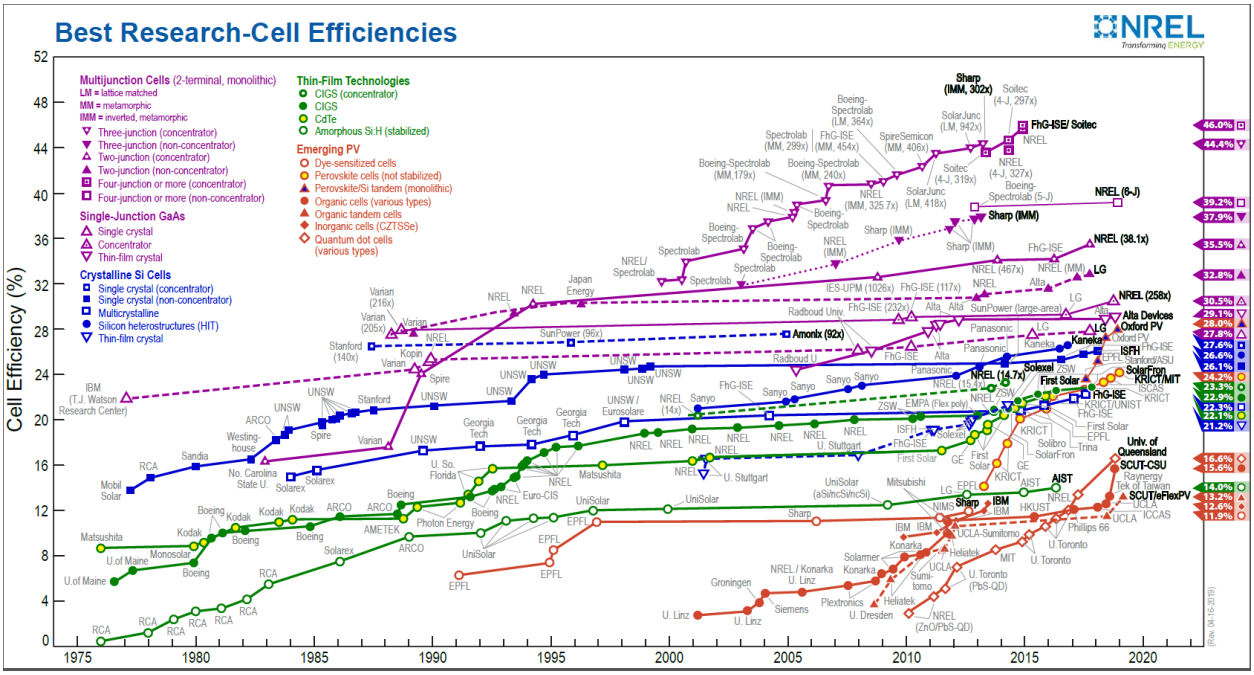

Figure 2.2.2: Highest energy conversion efficiencies of research solar cells determined by certified agencies and laboratories worldwide from 1976 through 2019 for various PV technologies.[21]

In order to determine the efficiency of a given MJSC, the *I-U* characteristic curve of a cell must first be determined. The *I-U* characteristics of the cell may be determined by measuring the current output of the cell by sweeping over a series of voltages. There are three main parameters, which provide information about the cell. The short circuit current (I_{SC}), the open circuit voltage (U_{OC}), and the maximum power point (MPP). The short circuit current is the current generated by the MJSC under illumination where there is no load on the cell (the applied voltage is zero). Conversely, the open circuit voltage occurs when there is no net current and the resistance is

infinite. The *MPP* is along the *I-U* curve where the product of the current and voltage is the greatest. The energy conversion efficiency of the solar cell η_{MJSC} may be calculated by:

$$\eta_{MJSC} = \frac{P_{out}}{P_{in}} \times 100\% \tag{16}$$

where P_{in} is the power input to the MJSC and P_{out} is the output power delivered by the MJSC in watts. When the solar cell is being practically used to harvest solar energy, P_{in} is the power input from the sun; however, in a laboratory setting, P_{in} is the power input from the light source. Similarly, the maximum energy conversion efficiency of the solar cell may be calculated by:

$$\eta_{MJSC,max} = \frac{MPP}{P_{in}} \times 100\% \tag{17}$$

By considering the *MPP*, open circuit voltage and short circuit current, an additional characteristic can be obtained known as the fill factor. The fill factor is the ratio of the *MPP* to the product of the open circuit voltage and the short circuit current and is given by:

$$FF = \frac{MPP}{U_{OC} I_{SC}} \tag{18}$$

The fill factor of the *I-U* curve will describe the shape of the *I-U* curve, the closer the fill factor is to one, the closer the *I-U* curve is to a rectangle. The fill factor can provide information about the performance of the cell and indicate if there are series and shunt parasitic resistances [22]. Parasitic series resistance is inherent and typically arises from the fabrication of the solar cell itself (typically at contact points between two materials), while shunt resistance is a result of manufacturing defects [15]. Series resistance will reduce the voltage value at the *MPP*, and shunt

resistance will reduce the current value of the *MPP*, both decreasing the overall efficiency of the cell.

Temperature greatly impacts solar cells as the band gap energy decreases with increasing temperature. The decrease in band gap energy results in an increase in thermalization losses reducing the solar cell's maximum energy conversion efficiency [23].

2.2.2 Solar energy spectra

The light energy released by the sun is a broad spectrum with wavelengths ranging from the nanometer to decimillimeter range. The greatest portion of solar irradiance is in the visible region with wavelengths between 300 nm to 800 nm. Before entering the Earth's atmosphere, the spectrum of solar irradiance is close to that of black body radiation at 5760 K; the temperature of the sun [13]. The spectrum of solar irradiance that reaches just before the Earth's atmosphere is referred to as the AM0 spectrum, where AM stands for air mass. As the solar irradiance enters the atmosphere, energy levels are reflected or absorbed to different extents so that the solar spectrum, which reaches the ground is different from the AM0 in both overall and individual wavelength intensity. The AM1.5 is the spectrum of the sun's irradiance, which reaches the Earth's surface between 0° and 48.2°, relative to the zenith. The terms AM0 and AM1.5 refer to reference spectra from the American Society for Testing and Materials (ASTM) [24]. The AM1.5 spectrum is further divided into AM1.5 Global (AM1.5 G) and AM1.5 Direct (AM1.5 D). AM1.5 G refers to irradiance that is both directly incident and diffuse from the sky and ground reflections where AM1.5 D refers to the irradiance that is only directly incident, and disregards diffuse irradiance from the sky and ground reflections. This distinction is necessary when considering light concentrating systems, which typically have a low acceptance angle. These spectra from the ASTM are displayed in Figure 2.2.3 where it can be visualized that AM0 is greater in overall intensity than AM1.5 G, which is greater in overall intensity than AM1.5 D. It can also be seen that the intensities for individual wavelengths vary between the spectra, but that the region of greatest intensity is consistently between 300 nm and 800 nm.

The total power density emitted by the sun is around $6.25 \times 10^{11} W\ m^{-2}$, which is reduced to only $1.367 \times 10^{3}\ W\ m^{-2}$ before the light enters Earth's atmosphere [25].The ASTM lists the

power density output of the AM1.5 D to be $7.633 \times 10^2\ W\ m^{-2}$ and the AM1.5 G as $9.638 \times 10^2\ W\ m^{-2}$.

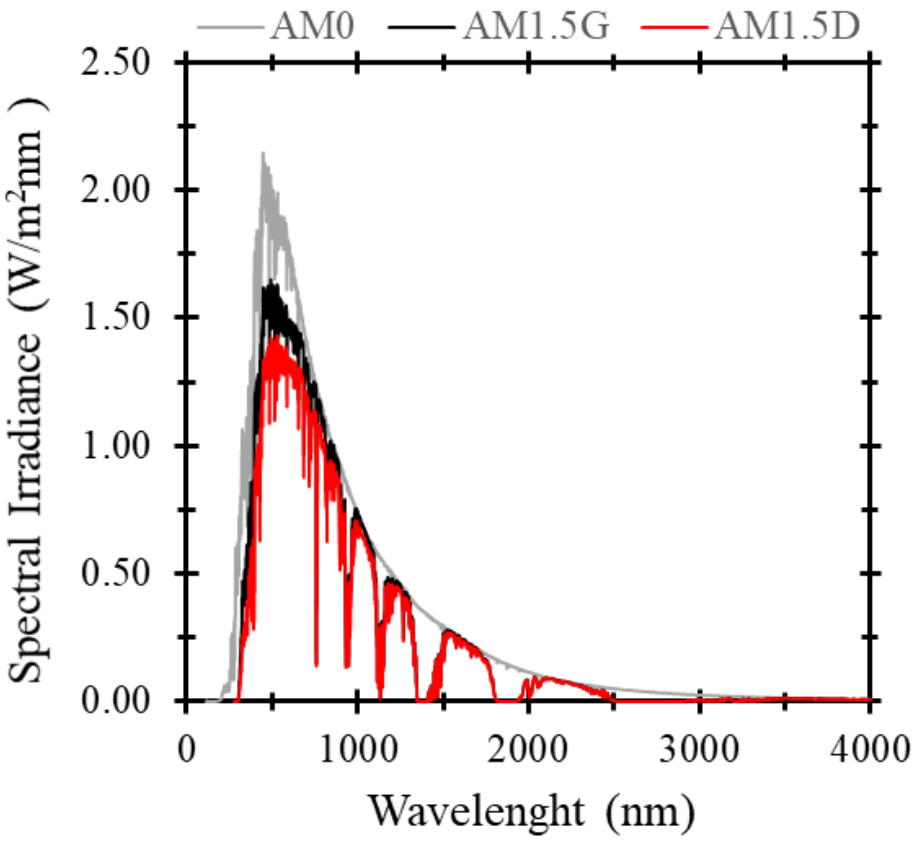

Figure 2.2.3: A selection of AM0, AM1.5G, and AM1.5 D solar spectra from ASTM[26][27].

2.3 The combined electrolyser PV system

Electrolyser PV systems combine the benefit of clean energy production from the sun with the convenience of the transportability and conversion flexibility of hydrogen gas [28]. In a combined electrolyser PV system, the PV cell harvests the naturally abundant energy of the sun to produce an electrical current, the electrical current may then be used to provide the electrical energy needed to drive the water electrolysis reaction in an electrolyser. This process was first presented in Figure 1.1.1. Methods to store renewable energies are essential for robust renewable energy systems as naturally occurring energy sources like solar energy are not always available. The hydrogen produced by the combined electrolyser PV system may provide energy to replace the energy derived from non-renewable energy sources on the grid, or provide electricity to remote, off-grid sites [12]. As combined electrolyser PV systems do not rely on carbon fuels, they do not directly emit carbon dioxide and other greenhouse gases. These systems also provide an improvement over battery storage of solar energy systems as batteries are composed of harsh components, which must be safely disposed of after their limited life cycle.

When considering practical installation of such a system, there are many factors, which must be considered including the siting of the solar panels, the cost of the system and ancillary components, and the efficiency of the system. Though it is clear that this zero-emission system is an environmental improvement, it is not yet widely commercially available because of the comparatively high cost of the system. As such, for this system to be commercially viable, advancements should be made to reduce the cost of the systems and ancillary components, and improve the efficiency of the system. The scope of this thesis was to develop methods and use these methods to measure the efficiency of a one-to-one MJSC to PEM electrolyser system in a laboratory setting.

2.3.1 Combined system configuration

In a one-to-one MJSC system to PEM electrolyser, the two components are electrically connected so that the current generated by the input of light energy to the MJSC, is the input current used to drive the electrolysis reaction in the electrolyser; the current output from the MJSC is the current input for the PEM electrolyser. The electrolyser puts a load on the system and the potential difference across the cell is the voltage applied to the MJSC. As the current and

voltage are directly related between the two systems, it is important to ensure that the current produced by the solar cell is an appropriate level for an input current for the PEM electrolyser and similarly, that the potential difference across the PEM electrolyser is an appropriate load for the solar cell. For example, a one-to-one electrolyser PV system utilizing a standard Si single junction solar cell is not an option as the open circuit voltage of such a solar cell is typically no more than 0.7 V [1], which is below the thermoneutral voltage of electrolysis. As the current and voltage are inherent to calculating efficiency of the two separate systems, they will therefore be inherent to the STH efficiency.

2.3.2 STH efficiency

The hydrogen production efficiency of any electrolyser PV systems is referred to as STH energy conversion efficiency. The STH efficiency is a product of the efficiencies of the PV system and the electrolyser. Since in this work the PV and electrolyser systems used were a MJSC and a PEM electrolyser, respectively, the STH efficiency is defined by the following equation:

$$\eta_{STH} = \eta_{PEM}\eta_{MJSC} \tag{19}$$

where $\eta_{PEM}$was first defined in equation (15) and η_{MJSC} was defined in equation (16). Looking at the two systems separately, modern MJSC under concentration can be realistically expected to have efficiencies around 35%, while PEM electrolyser systems are expected to have an efficiency of around 90% in a laboratory setting. As such, the overall STH energy conversion efficiency is significantly more limited by the comparatively low efficiency of the MJSC. Furthermore, MJSC are theorized to have a maximum potential efficiency under concentration of 86%, so there is room for significant improvement of the efficiency of the MJSC, which would then have a great impact on the overall STH efficiency.

Hydrogen generation from solar energy has been an area of significant research since the mid-nineties and earlier. Systems significantly vary from photothermal systems [29], photochemical monolithic devices [30] to coupled systems similar to the one used in this work [31]. In the most comparable work, a MJSC under concentration was directly connected to a PEM electrolyser. The MJSC has a theoretical energy conversion efficiency of 50%, though the experimental efficiencies only reached 30%. The overall measured STH efficiency was 18.1%, which at the

time was the highest reported STH efficiency to date. More recently, similar systems have reached STH efficiencies of 24.4% [32] and 30% [33].

Temperature of the combined system impacts both the efficiency of the MJSC and the PEM electrolyser. As temperature increases, the efficiency of the MJSC decreases as thermalization loses increase. In contrast, increasing temperature increases the efficiency of the PEM electrolyser as less potential difference across the cell is required to drive the dissociation reaction.

2.3.3 System matching

As the PV system supplies the electrical energy to the electrolyser, there is always the issue of an impedance mismatch between the load of the electrolyser and the electrical output characteristics of the PV system, as well as a mismatch between the optimum operation parameters of each respective system. As will be demonstrated in this work, the efficiency of each individual system is dependent on the input parameters. For example, the solar cell will function at a range of applied potentials, but has a single potential, which results in the greatest efficiency of the system. Similarly, there is a single input current, which will maximize the hydrogen production efficiency of the PEM electrolyser. As the ideal operating voltage of the PV system is unlikely to result in the exact optimum operation current for the electrolyser, and the load of the electrolyser is unlikely to result in the optimal potential of the PV system, both systems are unlikely to operate under ideal conditions when they are connected in a one-to-one system. This issue may be overcome through system optimization where multiples of each system are connected in series, or parallel so that the optimum operation conditions may be reached for each of the individual components of the combined system [34]. An alternate solution is the use of the DC-DC converter and *MPP* tracker may be used to ensure optimal power transfer between the two systems [12]. As the electrical characteristics of the PEM electrolyser are active cell area dependent, this issue of a system mismatch may also be addressed by changing the active area of the PEM electrolyser [31]; however, when using commercial systems, this solution is not always available or practical. Though system matching is essential for practical systems, this work aimed to study the one-to-one system using commercially available systems. The one-to-one

system would not operate at the maximum operation conditions, but still results in essential information for modeling and for developing a greater understanding of the individual systems.

3 Experimental Methods

3.1 Introduction

This section describes the experimental setups used for the determination of the energy conversion efficiencies of the MJSC, PEM electrolyser, and combined system. The procedures provided will be sufficient to replicate all experiments.

3.2 Equipment background

This section describes the experimental setups used for the determination of the MJSC, PEM electrolyser, and combined system energy conversion efficiencies. This section also details the functioning principals of the equipment and instrumentation used for this analysis.

3.2.1 Solar simulator

A Sol 3A solar simulator, model 94123A-CPV (Oriel Instruments, California, USA) was used to simulate irradiance from the sun. The Sol 3A uses a 1600 W arc lamp power supply, model 69922, (Oriel Instruments, California, USA), to ignite a xenon arc lamp, model 62726, which acts as the light source of the solar simulator. The irradiance produced by the xenon lamp is redirected by an ellipsoidal reflector and a primary mirror to a manually operated variable aperture accessory known as the partial sun attenuator, which adjusts the irradiance output. After the partial sun attenuator, the irradiance passes through a spectral correction filter so that the spectrum of the solar simulator better mimics the natural sunlight at the surface of the earth. Finally, the light is redirected with a secondary mirror through a collimating lens and onto the MJSC mounted on the stage. A representation of the light path through the solar simulator is

displayed in Figure 3.2.1. The working distance for the Sol 3A solar simulator is listed in the manual as 10.2 ± 1.3 cm, 11.4 cm was used for all experiments.

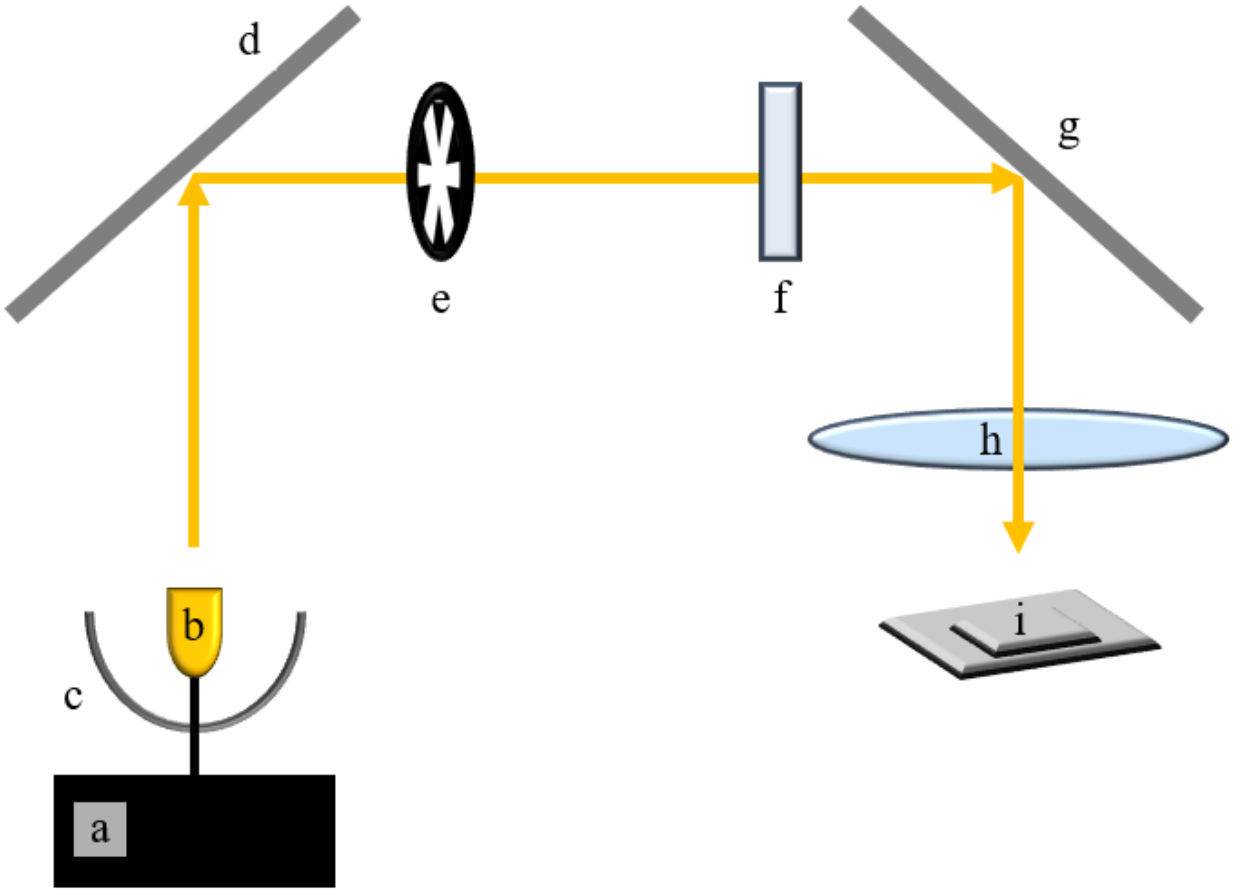

Figure 3.2.1: Schematic representation of the light origination and path through the solar simulator, the Sol 3A, to the test MJSC. A power supply (a) is used to ignite the xenon arc lamp (b). All of the irradiance produced from the xenon arc lamp is reflected and directed by the ellipsoid reflector (c) to the primary mirror (d). The primary mirror then redirects the output irradiance towards the partial sun attenuator (e). The partial sun attenuator may be manually opened or closed to alter the output irradiance, which then passes through a spectral filter (f), which alters the spectrum of irradiance. The output irradiance continues to a secondary mirror (g) and is redirected to a collimating lens (h) and finally, to the test MJSC.

The spectral correction filters used in the solar simulator are AM1.5 Direct and AM1.5 Global, models $81011^{*} + 81085$ and $81011^{*} + 810856$ respectively. These filters are used to alter the output irradiance from the solar simulator's xenon arc lamp to better replicate that of the solar spectrum at the Earth's surface. Since the solar concentrator systems used for solar cells have low acceptance angles, AM1.5 D is required when testing the performance of solar cells so that the diffuse irradiance is not contributing to the solar input to better reflect realistic conditions. ASTM lists the power density output of the AM1.5 D to be $763.3\ W\ m^{-2}$ and the AM1.5 G as

$963.8\ W\ m^{-2}$. The reference cell, effectively used to standardize the light intensity of the solar simulator, is calibrated so that the intensity of 1 Sun ($\Gamma_{1\ Sun}$) is equal to $1000\ W\ m^{-2}$ and is therefore the definition used for 1 Sun at $25°C$ in all presented results. The Sol 3A is a Class AAA solar simulator, indicating that the spectral match to the National Research Energy Laboratory (NREL) incident solar spectrum standard doesn't deviate beyond $0.75\% - 1.25\%$ of the ideal irradiance, the non-uniformity of the irradiance over the working area is $\leq 2\%$, and a has a temporal instability of $\leq 2\%$.

3.2.2 Source meters

Two source meters were used in the experimental set up, the Keithley Thermoelectric Cooler (TEC) Source Meter Unit, model 2510-AT and Keithley Source Meter Unit, model 2420 (Keithley, Ohio, USA). Both source meter units (referred to as SMUs) share the same main function; they supply a voltage and measure the resulting current, or supply a current and measure a resulting voltage, all done with greater accuracy than a general bench top power supply. SMUs are very easily programmable to meet a range of applications.

The Keithley TEC SMU was used in conjunction with an in-house prepared TEC system and is discussed in more detail in the temperature controller system section. The standard Keithley SMU was employed to obtain *I-U* characteristics of the test MJSC under varying levels of irradiance as well *I-U* characteristics of the PEM electrolyser. When used with the MJSC, the SMU was programmed to record the output current from the solar cell over a preset range of voltages. When studying the independent PEM electrolyser, the SMU supplied the current as would the MJSC in the combined system, and also recorded the voltage across the PEM electrolyser.

There are two Keithley SMU wire configurations used in this work; the two- and four-wire configurations. In the basic, two-wire configuration there is one wire for the positive and negative leads, in the four-wire configuration, there are two wires for each lead. The two-wire measurement is sufficient for measuring current as current is constant along a circuit in series. The two-wire configuration presents a problem when measuring voltage; the measured potential difference is the result of the resistance from both the device under test and the lead wires. In

order to circumvent this source of error, two additional connecting wires are added so that the resistance of the wires may be measured and accounted for.

Two laboratory developed software programs were used to interface between the Keithley SMU and the computer; one for measuring characteristics of the PEM electrolyser, and one for the MJSC. The software programs provided the SMU with the specific experimental parameters and allowed the computer to collect and record the data output from the SMU. These programs were originally developed by SUNLAB Postdoctoral fellow, Dr. Matthew Wilkins in both Python 2 and 3 programming languages. The programs were modified to meet the exact experimental conditions for the measurements performed in this work.

Though orders of magnitude more accurate than a general power supply, there are instrumental limitations of the Keithley SMU, which should be considered. When applying or measuring a voltage and current, the source and measured accuracy of the Keithley SMU is defined in the manual and the relevant accuracy values are later presented in the appendix, Table 6.1.1.

3.2.3 Temperature controller system

As the temperature of the solar cell has a significant impact on its performance [35], it was necessary to monitor and regulate the temperature of the solar cell under test during all measurements. As such, the desired temperature of the solar cell during all measurements was maintained with a temperature controller system, which was composed of a laboratory developed TEC stage regulated by a feedback loop between a $10\ k\Omega$ NTC Bead Head thermistor, model TCS610 (Wavelength Electronics, Montana, USA) and a Keithley TEC SMU. The TEC stage was attached to an aluminum block with conductive paste. A large fan was running next to the solar cell to provide additional cooling.

3.2.3.1 Thermoelectric Cooler

The Peltier effect is the core principal behind the TEC; when a current is passed through two dissimilar semiconductors, heat is either accumulated or lost at their junction [36]. This phenomenon is a result of heat transfer from charge carrier movement. P-type and n-type semiconductors are respectively defined by having holes and electrons as their principal charge carriers, and these charge carriers move oppositely to one another in response to a current; resultantly, heat is either accumulated or lost at their junction. In a TEC, many p-type and n-type

semiconductor couples are wired in series so that all junctions from which charge carries are moving towards are aligned on one side of the device, the “hot side”, and similarly, all junctions from which charge carries are moving away are aligned on the other side of the device, the “cool side”. A representative diagram of the equipment of this Peltier effect is represented in Figure 3.2.2. The aluminum block was attached to the “hot side” of the TEC with conductive paste. This aluminum block served the function of a heat sink, allowing the heat collected on the “hot side” of the TEC to more easily dissipate. Aluminum was chosen for this function as it has a low heat capacity and facilitates heat dissipation. Conductive paste was used to attach the TEC and the aluminum block to improve their contact and further the heat dissipation.

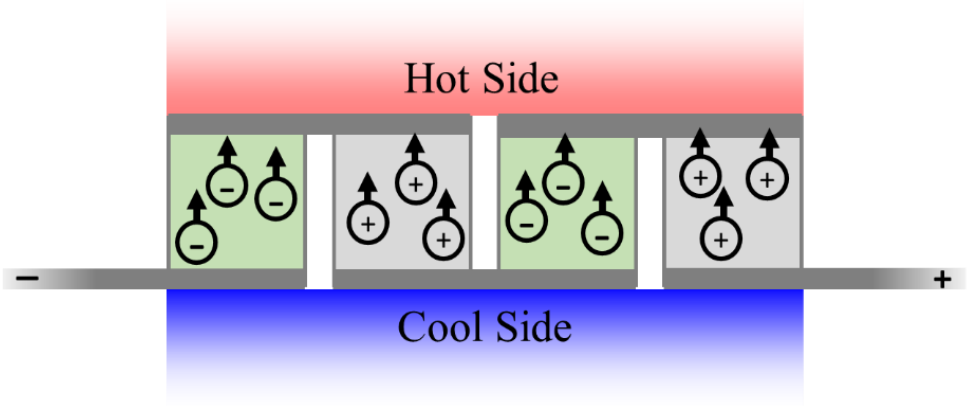

Figure 3.2.2: Schematic representation of the TEC system with two p-n junctions connected in series. The materials depicted in green and light grey are n-type and p-type semiconductors, respectively.

3.2.3.2 Thermistor

A thermistor, or a resistance thermometer, is based on the principle that the electrical resistance of a resistor is temperature dependent and allows the changes in the temperature of the resistor to be quantified by its change in resistance. The relationship between the electrical resistance of the resistor and its thermodynamic temperature is modeled by the Steinhart-Hart equation:

$$\frac{1}{T} = a + b(\ln \mathrm{r}) + c \ln^3 r \qquad (20)$$

Where a, b and c are the Steinhart-Hart coefficients and are device, and temperature range specific. r is the resistor’s resistance at temperature, T [37]. The Bead Head thermistor used in this project is a negative temperature coefficient type, polycrystalline semiconductor with 7.62 cm nickel wires that is rated to have a resistance of 10 $k\Omega$ at 25°C. The Keithley TEC SMU was

calibrated to the thermistor using the Steinhart-Hart coefficients provided by the manufacturer. The resistance of the thermistor is measured and the temperature is calculated and displayed by the Keithley TEC.

3.3 Electrolyser measurements

3.3.1 PEM electrolyser energy conversion efficiency

The Electrolyser 5 (H-TEC EDUCATION GmbH, Texas, USA) system consisted of a PEM electrolyser cell with two water reservoir/gas storage tanks. The electrolyser cell had an active surface area of 289 mm^2 and was composed of platinum loaded carbon paper as detailed by the manufacturer. The polymer electrolyte membrane within the cell had a thickness of 45 μm; its composition was unspecified. The maximum permissible operating voltage and current for the electrolyser cell were 2 V and 1.2 A respectively, and the gas storage tanks each had a maximum graded storage volume of 30 mL in 1 mL increments. Each water reservoir/gas storage tank was connected to the cell with two hoses. The gas tanks connected to the anode and cathode sides of the cell were for the collection of oxygen and hydrogen gas, respectively. A hose was attached to each of the gas tanks' outlets. The ends of the outlet hoses were initially clamped. The Keithley SMU was connected to the electrolyser cell in a four-wire configuration to account for the resistive loss of the wires and ensure accurate voltage measurements. See Figure 3.3.1 for the set-up configuration. To obtain the *I-U* characteristics of the electrolyser, the voltage was measured across the cell at a range of currents from 0.02 A, to 1.2 A at an increment of 0.02 A. The current was held constant for each respective measurement for the theoretical amount of time needed to produce 27.5 mL of hydrogen gas as per equation (21) in section 4.1.1. To perform these measurements, the water storage tanks were filled with roughly 50 mL of distilled water. Distilled water was used during the experiments so that the catalysts were not poisoned and to prevent any undesirable side reactions because of any contaminates that may be present in tap water. The hose clamps were released to allow the water to fill the gas storage tanks and the cell, and were then clamped again. The hose lines and cell were checked for bubbles. The in-house prepared software and Keithley SMU were used to apply the desired current and concurrently measured the applied current and potential difference across the electrolyser cell over time. The gradations on the side of the gas storage tanks were used to measure the volume of produced hydrogen. See Figure 3.3.1 for an image of the gas storage tanks without and with

10 mL of hydrogen gas. These measurements were performed at eye level on a level surface. All volume measurements were rounded to the nearest lower half integer leading to a measurements error of ± 0.25 mL. See Figure 3.3.2 for the gas storage tanks without (a) and with (b) 10 mL of hydrogen gas. The pressure and temperature of the closed system were assumed to be 1 atm and $25°C$. This series of experiments was repeated in duplicate.

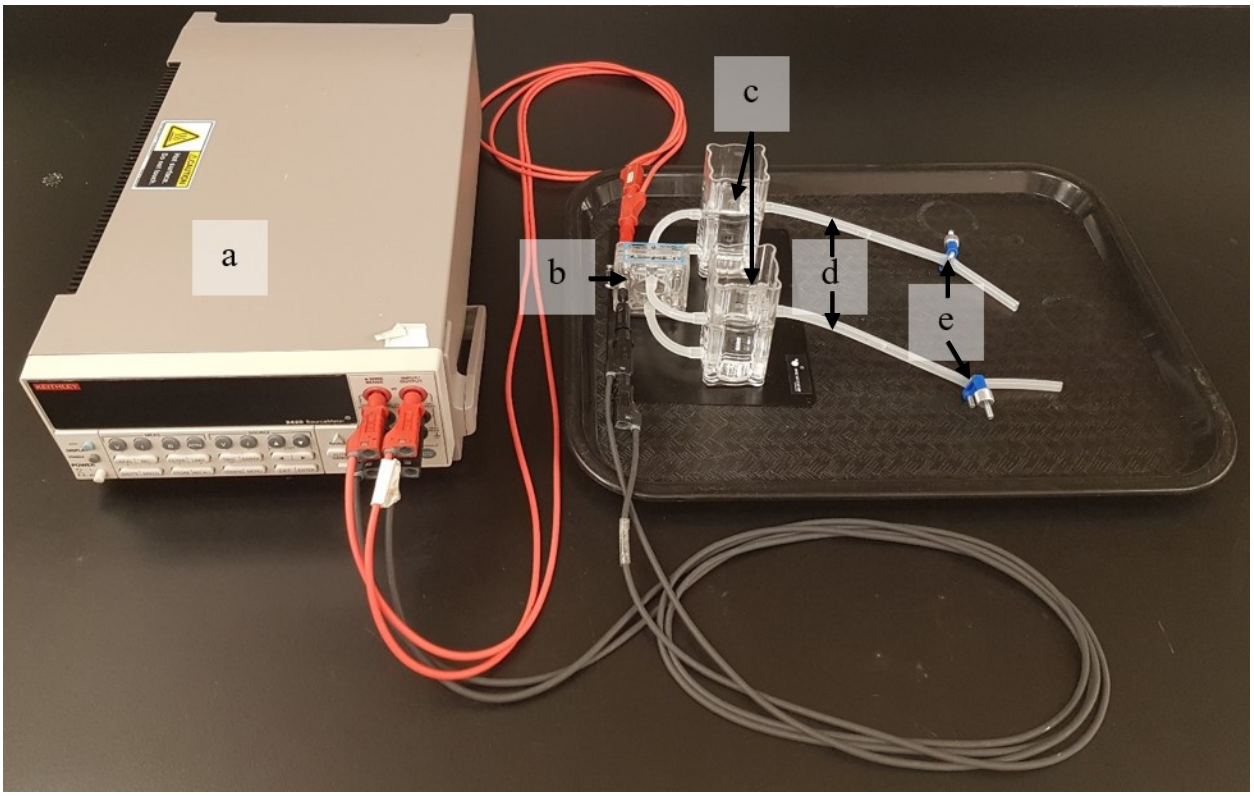

Figure 3.3.1: PEM electrolyser set up used to measure the energy conversion efficiency of the PEM electrolyser. The system consists of a) a Keithley SMU 2420, b) a PEM electrolyser cell, c) two water reservoir/gas storage tanks, d) two outlet hoses for water and gas expulsion and e) two hose clamps. During measurements, the Keithley SMU 2420 would be connected with a computer and the in-house prepared software was used to apply the desired current and concurrently measure the applied current and potential difference across the electrolyser cell over a predetermined period of time.

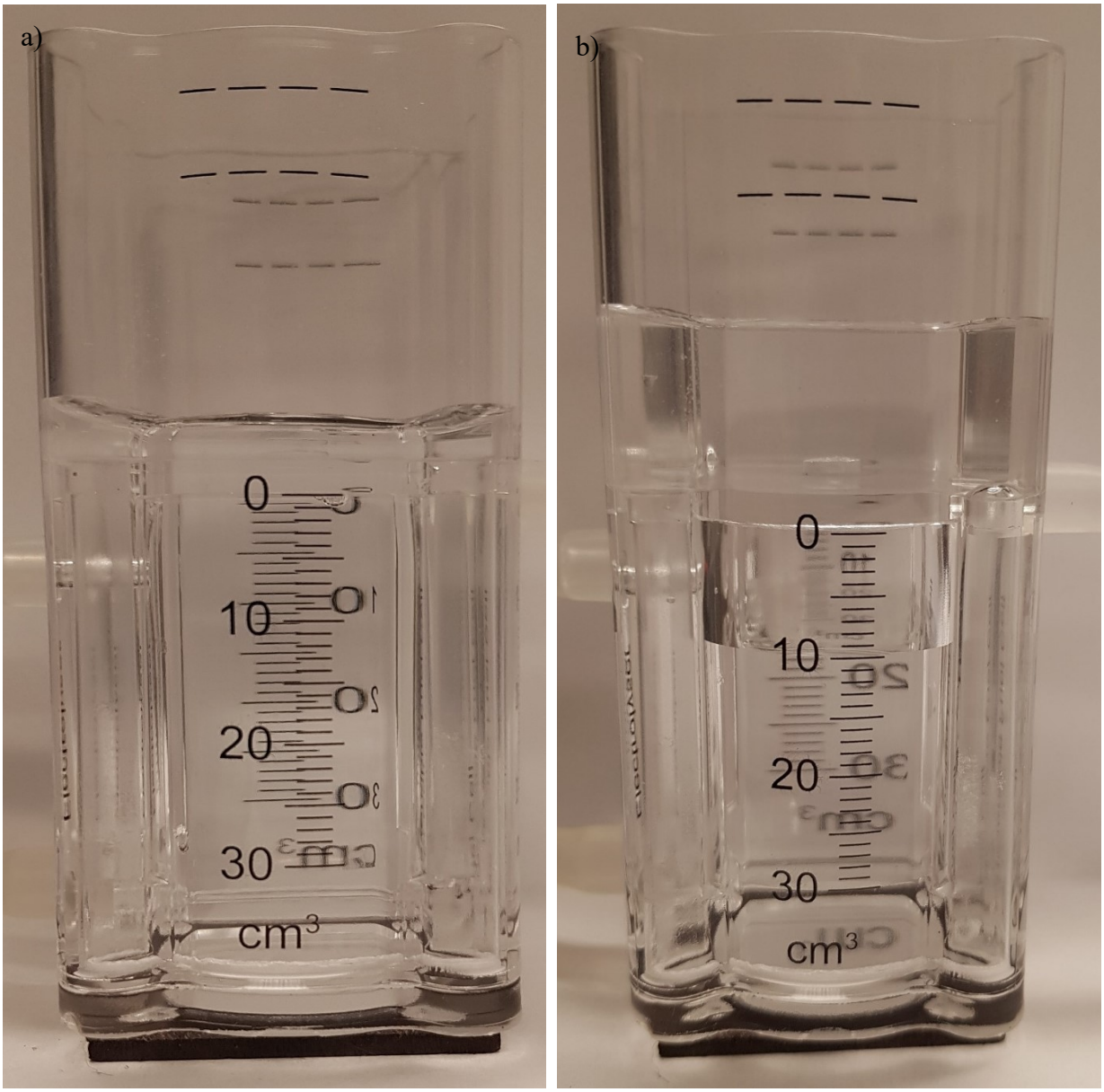

Figure 3.3.2: Water reservoir/gas storage tank for the PEM electrolyser, which was used to determine the volume of gas produced over a set period of time. The water reservoir/gas storage tank of the PEM electrolyser is presented a) with no hydrogen b) with 10 mL hydrogen.

3.4 Solar measurements

3.4.1 General conditions

The solar simulator was turned on for 30 minutes prior to each measurement to allow the light source to stabilize as recommended by the Sol 3A manual. The temperature of the MJSC under investigation was maintained at 25°C for all measurements, regulated by the temperature

controller system. Once the cell under investigation was placed on the stage, the temperature of the cell as displayed by the Keithley TEC SMU was allowed to stabilize, which took approximately 5 minutes, but up to 12 minutes for the highest solar concentrations. The height of the stage was adjusted so that the separation distance between the test cell and the lowest most part of the solar simulator was 11.4 cm.

3.4.2 Determination of one Sun short circuit current for the test MJSC

The test MJSC used was a 1 cm by 1 cm InGaP/(In)GaAs/Ge MJSC (Cyrium Technologies Inc., Ontario Canada). The light source used was the Sol 3A solar simulator, with the company-provided AM1.5 G filter and collimated lens. In order to measure the irradiance output strength of the solar simulator, a PV Reference Cell System, model 91150V (Oriel Instruments, California, USA) was used. This system consists of a 2 cm by 2 cm monocrystalline silicon PV reference cell and a display meter. This system measures and displays the solar irradiance incident on the reference cell in the unit "Suns". This unit is based on the expected direct normal irradiance incident on the Earth's surface from the sun and is equivalent to 1000 W m^{-2}. The irradiance measurement is the energy input value for the determination of the energy conversion efficiency of the solar cell.

After the solar simulator's 30-minute stabilization period, the reference cell was placed on the stage so that the cell was in intimate contact with the thermistor to ensure accurate temperature measurements. The partial sun attenuator was adjusted so that the irradiance output of the solar simulator was 0.5 Suns, as displayed by the reference cell display meter.

The reference cell was removed, and under identical conditions, the test MJSC was placed on the stage. The test MJSC was connected to the Keithley SMU with the two-wire configuration. The current generated by the MJSC when no voltage was applied was measured. This short circuit current was multiplied by two to obtain the 1 Sun short circuit current for the MJSC. This

measurement was repeated five times. Figure 3.4.1 displays a photo of the general equipment set-up.

For the remaining solar characterization experiments, the test cell was placed on the stage under identical conditions and the partial sun attenuator was adjusted to the desired irradiance output based on the measured the short circuit current for 1 Sun.

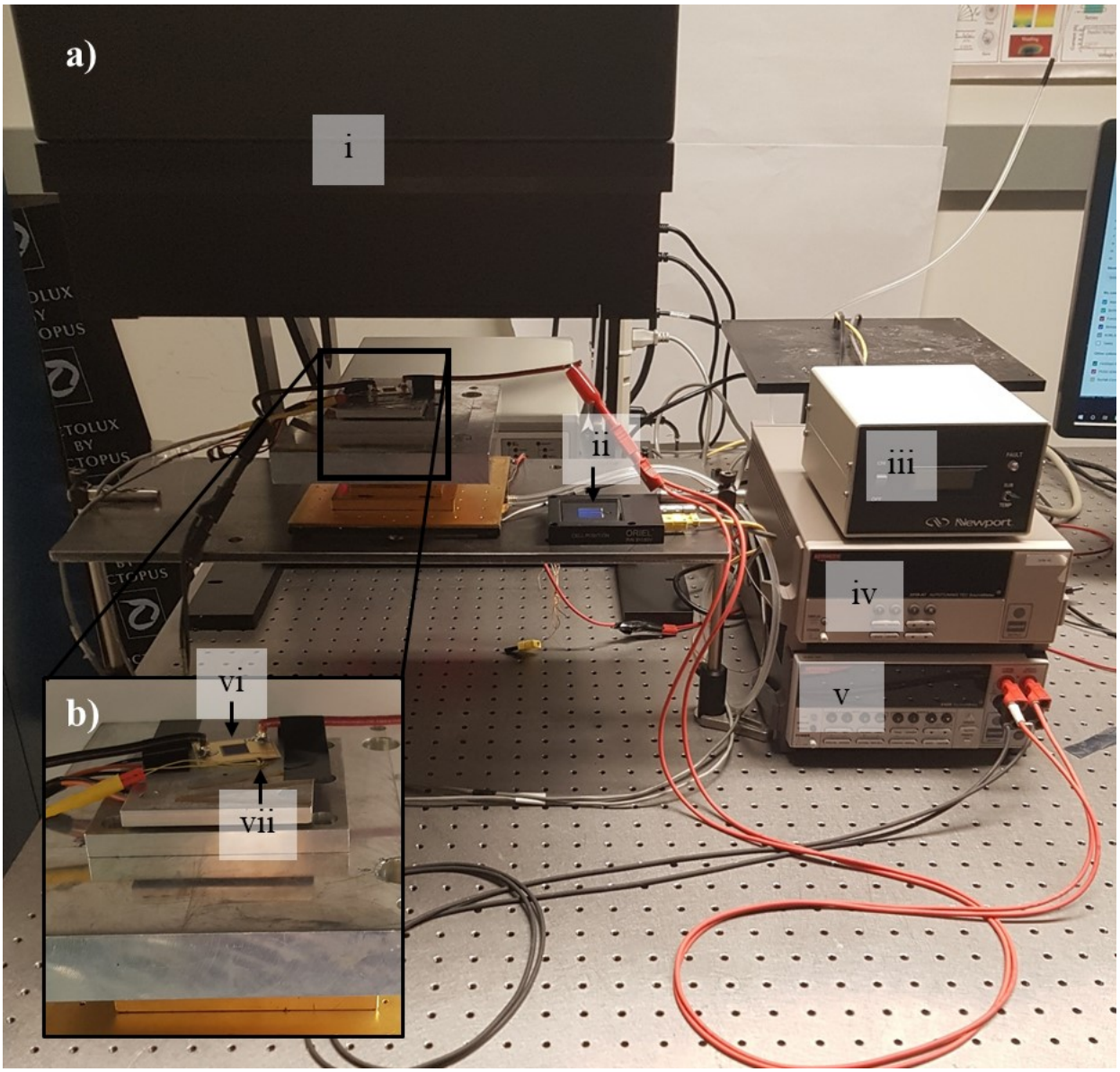

Figure 3.4.1: a) Laboratory set up used to measure the energy conversion efficiency of the MJSC and b) a close up of the MJSC. The system consists of i) a Sol 3A solar simulator, ii) a PV reference cell, iii) a PV reference cell meter, iv) a Keithley TEC 2510-AT SMU, v) a Keithley SMU 2420, vi) a MJSC and vii) a 10 $k\Omega$ NTC Bead Head Thermistor. The MJSC and Thermistor are sitting on the laboratory developed TEC. The cooling fan is placed to the left of the photo. When being used, the reference cell would be placed on the stage where the test cell is in the photo.

3.4.3 Multi-junction solar cell energy conversion efficiency measurements

The test MJSC was placed on the stage under identical conditions as the 1 Sun short circuit determination measurements, except the AM1.5 Global filter was replaced with an AM1.5 Direct filter. The intensity of the irradiance from the solar simulator was adjusted to 0.5 Suns, 1 Sun, 5 Suns, 10 Suns, 15 Suns, 20 Suns, 25 Suns and 30 Suns. In order to reach solar concentrations above 0.9 Suns, a Fresnel lens was added to the solar simulator after the collimating lens. The Fresnel lens is plexiglass with concentric grooves, which focus the incident collimated irradiance onto the MJSC, as displayed in Figure 3.4.2, and served the function of increasing the irradiance incident on the MJSC.

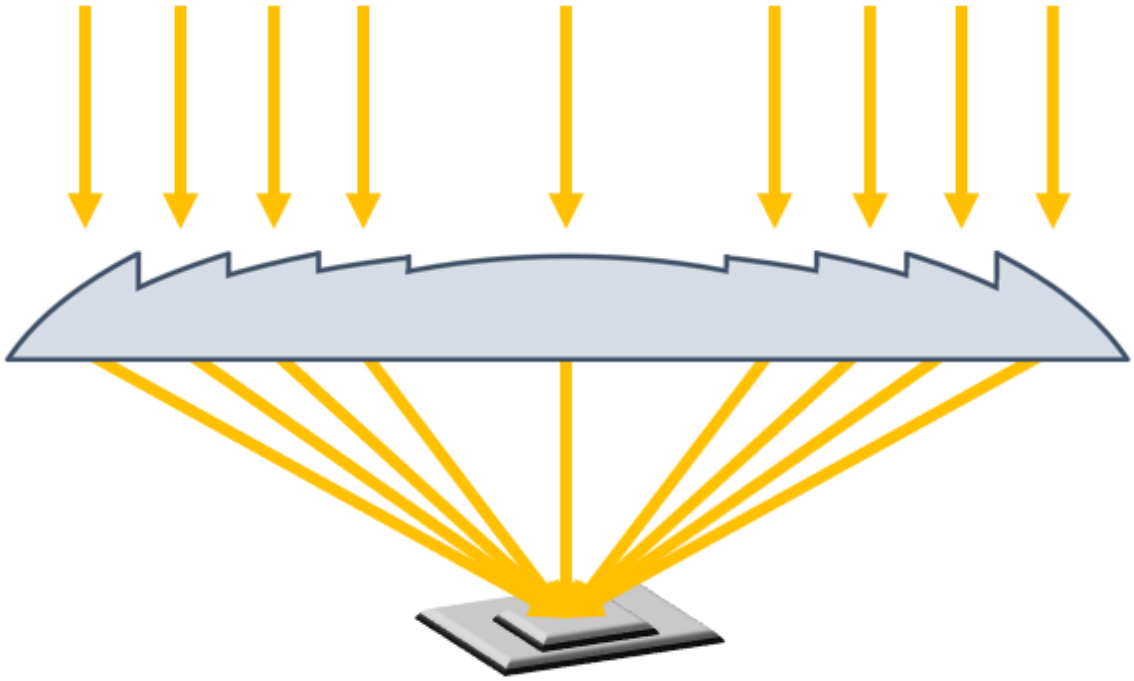

Figure 3.4.2: Previously columnated irradiance is concentrated towards the surface of the test MJSC by use of a Fresnel lens.

Once the desired irradiance was obtained, the connection between the MJSC and the Keithley SMU was changed from a two-wire configuration to a four-wire configuration. Using the laboratory developed software, the Keithley SMU ran the *I-U* curve protocol, which instructed the SMU to measure the current output from the MJSC over a voltage sweep from 0 V to 5 V at an increment step size of 0.01 V. Information on the *MPP* of the MJSC was determined at each

solar concentration from the obtained *I-U* curves and was used to measure the energy conversion efficiency of the test MJSC.

3.5 Combined system

3.5.1 STH energy conversion efficiency

The combined efficiency measurements were set up to mimic but combine the individual experimental set ups for the test MJSC and the PEM electrolyser. The solar simulator was set up with the AM1.5 D filter and the Fresnel lens placed 11.4 cm below the solar simulators and was turned on for 30 minutes prior to each measurement. The temperature of the MJSC was maintained at 25°C for all measurements regulated by the temperature controller system. The temperature was allowed to stabilize prior to each measurement. The test MJSC was placed on the stage in a two-wire configuration with the Keithley SMU. Based on the short circuit current displayed by the Keithley SMU, the intensity of the irradiance from the solar simulator was adjusted to the desired solar concentration.

The PEM electrolyser was prepared identically to the previously described tests in that roughly 50 mL of deionized water was poured into the water reservoir, the exit tubes were momentarily opened to allow the water to fill the cell and the gas capture vessel before the tubes were closed again. The line was inspected to ensure there were no gas bubbles. Rather than connecting the PEM electrolyser to the Keithley SMU, the PEM electrolyser was connected to the test MJSC as the current source. See Figure 3.5.1 for the instrument and equipment set up.

Six (6) trials were carried out and were reproduced in triplicate at 5 Suns, 10 Suns, 15 Suns, 20 Suns, 25 Suns, and 30 Suns. The time that the PEM electrolyser and test MJSC were connected was based on the output current produced by the solar cell at these 6 solar concentrations when connected to the PEM electrolyser and the resulting time required to produce 27.5 mL of

hydrogen gas as per equation (21) in section 4.1.1. After each trial, the amount of hydrogen and oxygen gas produced was measured.

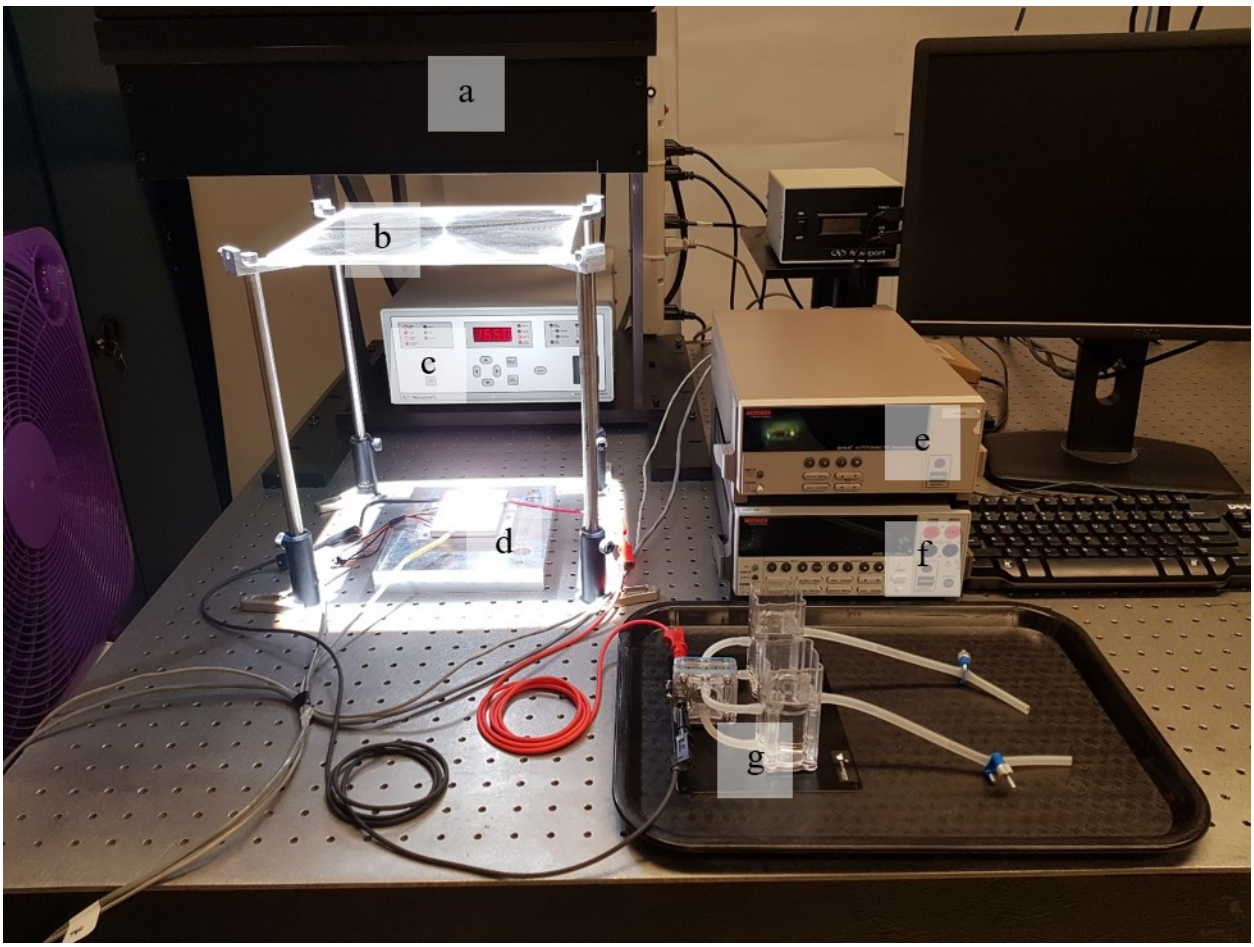

Figure 3.5.1: The instrument and equipment configuration of the combined MJSC and PEM electrolyser system used to measure the STH energy conversion efficiency. The necessary equipment and instrumentation to measure the efficiency consisted of a) a Sol 3A solar simulator, b) a Fresnel lens, c) a 1600 W arc lamp power supply, d) a MJSC on the temperature control system, e) a Keithley TEC 2510-AT SMU, f) a Keithley SMU 2420, and g) an Electrolyser 5 electrolyser system.

4 Results and Analysis

4.1 PEM electrolyser

In order to determine the practical STH energy conversion efficiency of a MJSC PEM electrolyser system, it was first necessary to identify the optimum operating conditions in a laboratory setting of the PEM electrolyser. In the combined system, the MJSC supplies the current to the electrolyser; in order to determine the desired current output for the MJSC, it was first necessary to measure and determine what current input range to the PEM electrolyser resulted in the greatest energy conversion efficiency. To accomplish this, the electrolyser was tested over a broad range of currents and experimental parameters were collected in order to determine, which currents resulted in an energy conversion efficiency equal to or greater than 90%, which was considered to be the optimal range. Using 90% as a benchmark for optimal energy conversion efficiencies is reasonable since it is routinely achieved in other comparable works [10].

To ensure that the optimal operation range of the electrolyser was encompassed by the range of tested currents, the entire possible range of currents was studied: as outlined by the manufacturer, the electrolyser system does not function below 0.02 A and is damaged at currents higher than 1.2 A. As such, this was the range selected to determine the optimal operation condition range. In order to obtain sufficient datapoints within that range, a step size of 0.02 A was selected for a total of 60 tested currents.

4.1.1 Theoretical production of hydrogen gas

Prior to each experiment at one of the 60 test currents, the theoretical time needed to produce 27.5 mL of hydrogen gas was calculated for each test current. A volume of 27.5 mL was chosen as the target volume of hydrogen gas as a result of the size and gradation on the gas storage tanks. The hydrogen gas storage tank had a maximum capacity of 30 mL with limited gradations so that the measurement error was estimated to be $\pm$ 0.25 mL. It was desired to have a measurement percentage error of less than 1% so 27.5 mL was selected as the target volume. The

time needed to theoretically produce 27.5 mL of hydrogen gas at SATP was calculated by rearranging equation (13) to solve for time,

$$t = \frac{z\,F\,V_{H_2 theoretical}}{I\,V_m} \tag{21}$$

Where $V_{H_2 theoretical}$ was set to 0.0275 L and I was set as the current used for each respective test. For this method to be valid, the assumption is made that the current efficiency of the theoretical production of hydrogen is 100%.

A sample calculation determining the theoretical time needed to produce 27.5 mL of hydrogen assuming a current efficiency of 100% at 1.0 A is as follows:

$$t = \frac{(2)(96485.33\ \text{s A mol}^{-1})(0.0275\ \text{L})}{(1.0\ \text{A})\ (0.0245\ \text{L mol}^{-1})}$$

$$t = 216\ \text{s}$$

Therefore, if the PEM electrolyser had a current efficiency of 100%, in that all electrons are used to produce hydrogen gas, it would take 216 s to produce 27.5 mL of hydrogen gas. This calculation was carried out for each input current prior to all measurements and the resulting times required to produce 27.5 mL of hydrogen gas at each respective current are summarized in Figure 4.1.1 below, as well as Table 6.2.1 in the Appendix. Figure 4.1.1 also allows for the

visualization of the exponential decay relationship between the time and input current as per in equation (21).

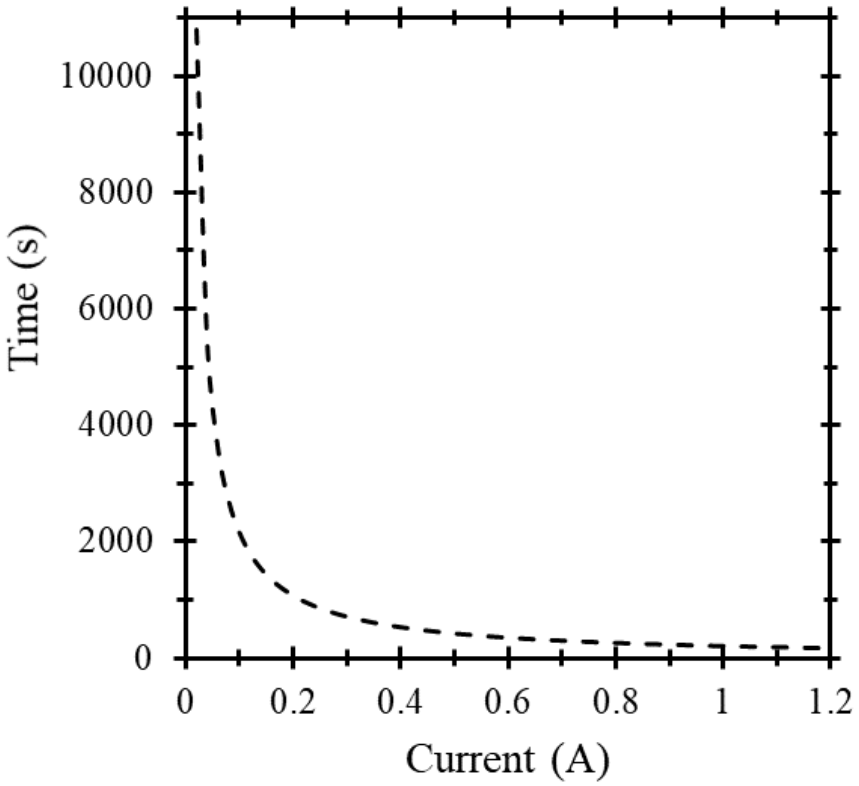

Figure 4.1.1: Time required to produce 27.5 mL of hydrogen gas with the PEM electrolyser assuming a 100% current efficiency.

4.1.2 Voltage-time measurements

When the PEM electrolyser was operating at each constant input current, the potential difference across the cell was measured every second over the duration of the experiment for all 60 test currents. Of the 60 test currents, a representative selection of the resulting voltage-time graphs is displayed in Figure 4.1.2. As the duration of the experiments at each of the 60 currents drastically varied, the time is graphed on a logarithmic scale. From Figure 4.1.2 it is clear that the time needed to reach the thermoneutral voltage, 1.48 V, was greater for the lower currents studied. In order for the charge transfer reaction at the electrodes to occur, there needs to be a charge accumulation at each electrode; at higher currents, this charge accumulation is achieved in a shorter period of time [38]. For example, when the input current was 0.02 A, 0.2 A and 1.2 A, the cell took 65 s, 7 s and <1 s to reach 1.48 V, respectively. It is important to consider the potential impact that this delay to accumulate a sufficient potential difference capable of splitting water may have on the efficiency measurements. When calculating the theoretical production of hydrogen gas, it is assumed that hydrogen is produced for the entire duration of the test. In practice, for the lower currents, a portion of time was used to develop a sufficient charge accumulation on the surface of the electrodes, making the time used to calculate the theoretical production of hydrogen gas larger than the actual time. Fortunately, the time effectively wasted was always less than 2% of the total time and had a negligible impact on the results. Though the logarithmic scale was necessary to show the differences in the initial voltages between trials in Figure 4.1.2, the time required to reach a sufficient potential difference is exaggerated, as is the irregular shape of the trial at 0.02 A.

In order to later obtain the *I-U* characteristics of the electrolyser and measure the cell's efficiency, an average voltage (the operating voltage) was measured for each current test. To determine the average voltage for each test, only the voltages were considered after the cell collected a sufficient charge accumulation and stabilized as visualized by the "plateau" of each current test in Figure 4.1.2. This method of measuring averages was chosen because it was the best representation of the entire test's average voltage. The average voltage is summarized in Table 6.2.1 in the Appendix. At the end of each test, the final volume of produced hydrogen and oxygen were recorded to later assess the purity of the gases.

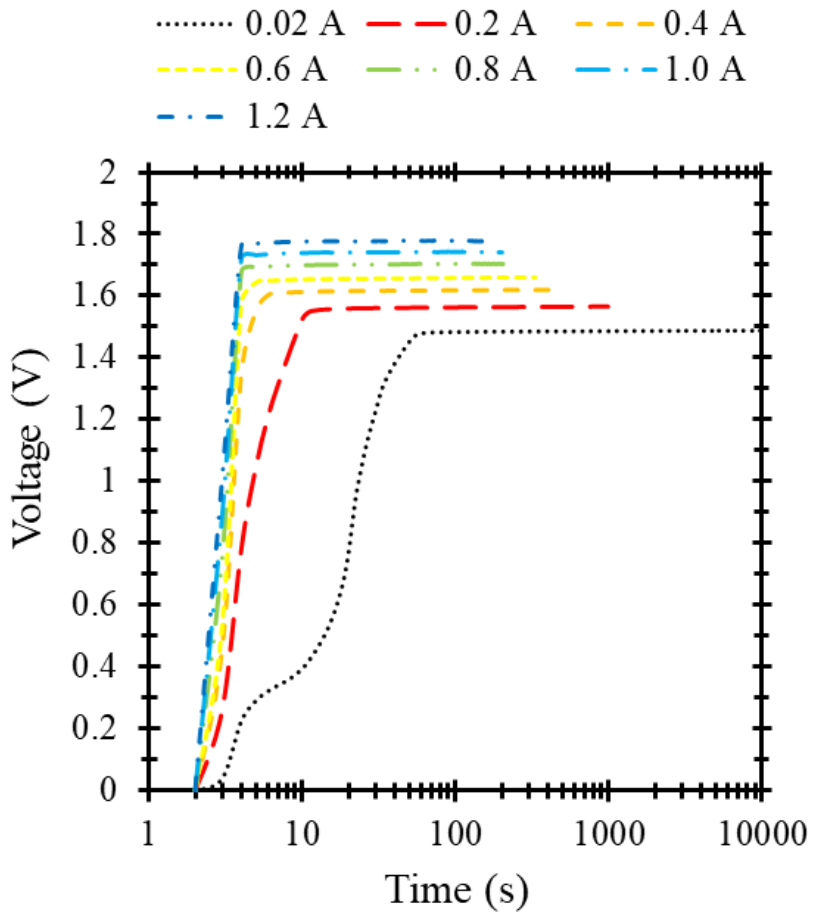

Figure 4.1.2: Measured voltage across the PEM electrolyser while under an applied current at 7 of the 60 tested input currents.

4.1.3 Energy conversion efficiency of the PEM electrolyser

The next characteristic of the PEM electrolyser, which was evaluated was its energy conversion efficiency. The energy conversion efficiency of the PEM electrolyser is a product of both its electrical and voltage efficiencies. The electrical efficiency, also known as the Faraday efficiency, is a measure of the percentage of the applied current, which is used towards the reaction of water into H_2 and O_2 gas and is first presented in equation (15). The voltage efficiency is simply a measure of what percentage of the voltage is greater than the

thermoneutral voltage; any voltage greater than the thermoneutral voltage is essentially wasted voltage.

In order to gain a full understanding of the efficiency of the system, the overall energy conversion efficiency is plotted alongside its two components, the current efficiency and the voltage efficiency, at each of the 60 tested currents in Figure 4.1.3. The target benchmark value of 90% for the overall energy conversion efficiency is also represented on the graph. At low currents, the Faraday efficiency has the largest impact on the overall energy conversion efficiency. Conversely, the voltage efficiency principally limits the energy conversion efficiency at larger test currents.

The voltage efficiency decreases with increasing current; the highest efficiency, 99.6% occurred at the lowest current tested, 0.02 A, and the lowest efficiency, 83.3% occurred at the highest current tested, 1.2 A. This trend is observed due to the relationship between current and voltage; as current increases, so does the voltage, and anything over 1.48 V decreases the voltage efficiency of the test.

The Faraday efficiency increases at a decreasing rate until it plateaus at 0.18 A after which the efficiency value remains around 98.5%. This indicates that in a given trial where the current is above 0.18 A, roughly 98.5% of the electrons are being used in the electrochemical reaction to produce hydrogen gas. There are many factors, which contribute to the electrical efficiency being lower than 100%. Parasitic reactions can occur from the presence of foreign atoms or corrosion/oxidation of components of the PEM electrolyser. Gas permeation through the proton exchange membrane may occur and reduce the current efficiency. Current leakage resulting from lattice or manufacturing defects may also be occurring and reducing the current efficiency [10]. These phenomena are more prominent at the lower range of test currents as there are fewer electrons and therefore a larger proportion of electrons are being lost to any or all of these phenomena [32]. At higher currents, the efficiency is limited due to the Joule effect. The Joule effect is the loss of electrical energy due to the formation of heat from the electric current circulating through the conductive material, which is more predominant at higher currents. Faraday efficiencies may also decrease as a result as gas leakages [39].

The overall energy conversion efficiency measures the efficiency to which electrical energy is converted into chemical potential energy. The current and voltage efficiencies cross at 0.140 A;

at currents smaller than 0.140 A, the efficiency is principally limited by the faradaic factors and above 0.140 A, the efficiency is limited by the increasing overpotential of the system. The greatest efficiency is achieved at 0.180 A and is 93.7%. The range of currents, which result in an energy conversion efficiency greater or equal to 90% is 0.060 A to 0.440 A.

This measured energy conversion efficiency of the PEM electrolyser is comparable to the reported efficiencies of similar systems. Efficiencies of PEM electrolysers have been theorized to be as high as 95% [28]. At a current input of 1 A cm^{-2}, Millet et al. reported an efficiency of 85% and noted that higher pressure and temperature will increase the efficiency of the electrolyser [40]. In a recent work evaluating the effectiveness of hybrid nanocatalysts, an efficiency of 93% was obtained at a higher current rate, 1.1 A cm^{-2} at 80°C [11]. As listed in

Table 6.2.1 in the appendix, the efficiency of the PEM electrolyser under evaluation in this work was measured to have an efficiency of 83.7% at 1 A.

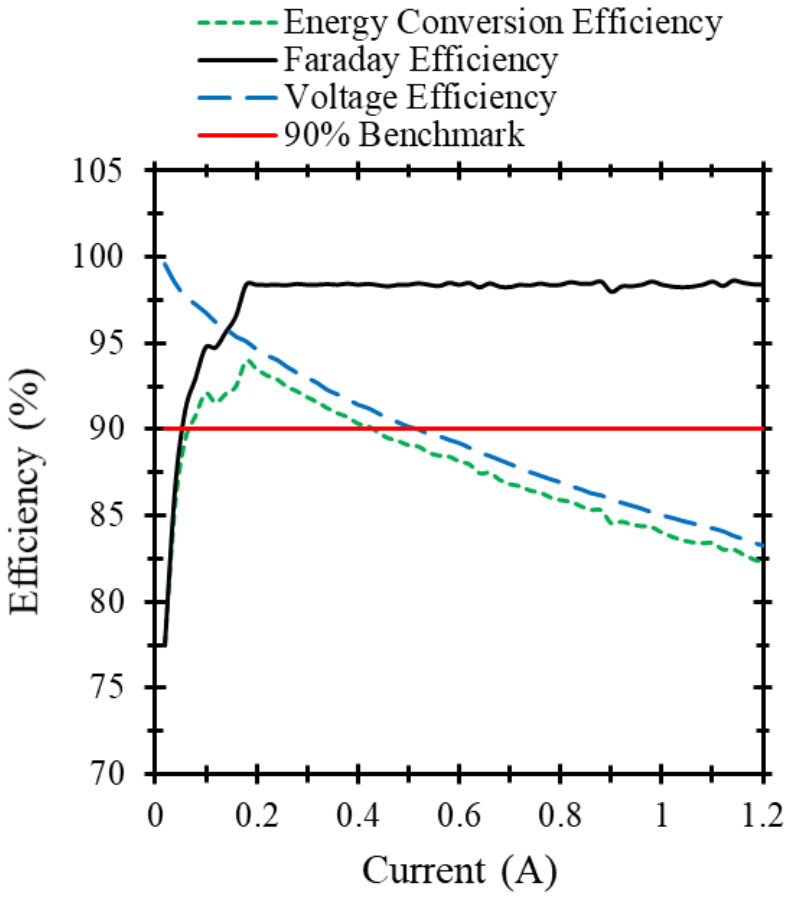

Figure 4.1.3: Faraday, voltage, and overall energy conversion efficiency of the PEM electrolyser.

4.1.4 Experimental set up evaluation

In order to evaluate the effectiveness of the experimental set up, the obtained efficiency results were compared to the technical data provided by the manufacturer. The manufacturer of the PEM electrolyser stated that at a single rated power input of 1.16 W, the average hydrogen gas production rate is 5 mL min^{-1}. They reported that this was an average hydrogen output, and that higher or lower production rates may also be achieved. Looking to equation (15), the

manufacturer reported efficiency of the cell may be calculated using this data point. Equation (15) stated that:

$$\eta_{PEM} = \frac{HHV\ V_{H_2 experimental}}{U_{op}\mathrm{I_{op}} t V_m}$$

The manufacturer listed the below information in the technical data sheet:

$$V_{H_2 experimental} = 0.005\ \mathrm{L}$$

$$t = 60\ \mathrm{s}$$

$$U_{op} I_{op} = 1.16\ \mathrm{W}$$

HHV and V_m for hydrogen are well known constants at SATP:

$$HHV = \ 285.84\ \mathrm{kJ\ mol^{-1}}$$

$$V_m = \ 24.5\ \mathrm{L\ mol^{-1}}$$

$$\eta_{PEM} = \frac{285.84\ \mathrm{kJ\ mol^{-1}}(0.005\ \mathrm{L})}{1.16\ \mathrm{W}\ (60\ \mathrm{s})(\ 24.5\ \mathrm{L\ mol^{-1}})} = 84\%$$

Given the above, based on the manufacturer reported performance of the electrolyser at SATP when the power input is 1.16 W, the efficiency is 84%. Of the 60 test currents in this work, the trial which is most comparable to a power input of 1.16 W is the trial at 0.680 A and 1.678 V and a power input of 1.18 W. Under these conditions, the efficiency was measured to be 86.8%. As this value is close, but above the average cell efficiency determined based off of the manufacturer reported performance characteristics of the electrolyser, it can be determined that the experimental set up is effective and the cell is operating as expected.

4.1.5 Polarization curve of the PEM electrolyser

The final characteristic of the PEM electrolyser evaluated in this work was its *I-U* characteristics by use of a polarization curve. A typical polarization curve for a PEM electrolyser is a plot of the average potential voltage across the cell against the applied current density during the duration of the experiment. In this work, the surface area of the electrolyser was 289 mm^2 so both the current

and current density are known. It was chosen to use current and not current density to present the *I-U* voltage characteristics because when compared to the *I-U* characteristics of the MJSC in which current is used, the two will be more comparable.

The polarization curve for the PEM electrolyser under investigation is presented in Figure 4.1.4. The voltage initially has a logarithmic response to increasing current, which gradually decreased in rate to a linear relationship to current around 0.300 A. The initial logarithmic region is referred to as the activation region, which is principally the overpotentials of the activation energies of the electrochemical reactions occurring on the surface of the anode [41]. Additionally, according to Fick's first law of diffusion, the flow of gas, i.e. the solubility of hydrogen gas into the solid electrolyte, is constant due to the constant thickness of the electrolyte. At low currents, the relative weight of the parasitic cross-over therefore dominates [42]. The linear portion is the ohmic region in which the limiting factor is the resistance the ions face as they migrate through the components of the electrolyser cell [43]. As the performance and overpotential of the electrolyser depend on the temperature of the cell [44], any small influxes in temperature will have an impact on the resulting polarization curve. The small, almost periodic deviances from a linear relationship in the ohmic region of the polarization curve is likely a result of changes to the ambient temperature of the cell's surrounding area. These deviances are small and do not impact the overall trend of the polarization curve. Above the currents studied, there would be a third region referred to as the concentration region; however, due to the limitation of the range of acceptable currents detailed by the manufacturer, the concentration region was not reached. The overpotential in the concentration region is principally a result of the decreased concentration of reactants at the surface of the electrodes, which occurs because there is a limit to the speed of which ions may flow through the electrolyte [43].

The relationship between the current and voltage of the electrolyser was needed when performing the combined system measurements because the voltage of the electrolyser could not be measured during the combined trials; this will be discussed in more detail in section 4.3. The *I-U* characteristics of the PEM electrolyser is a key piece of information in order to develop

combined systems, which operate at the *MPP* of the PV cell, which is necessary to develop a realistic system.

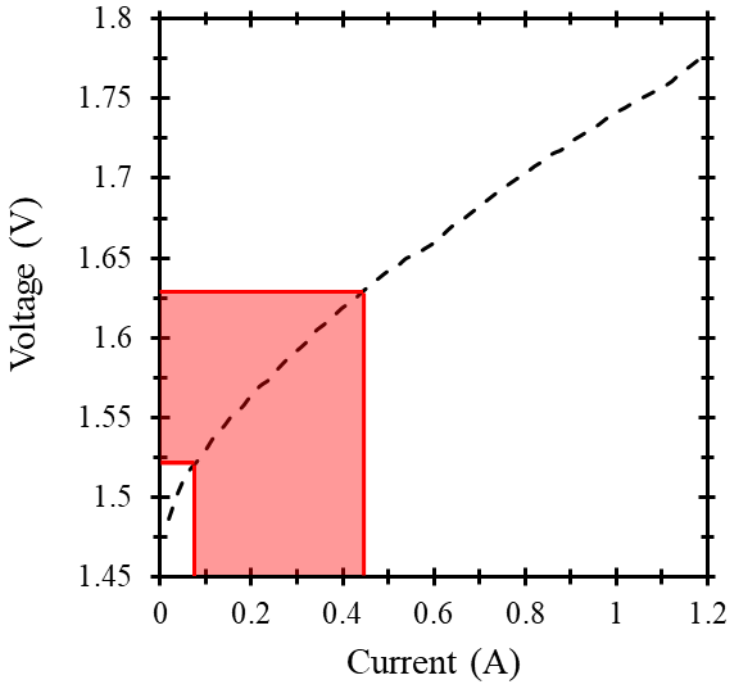

Figure 4.1.4: Polarization curve of the PEM electrolyser. The area in red identifies the area that results in an energy conversion efficiency of 90% or more.

4.1.6 Purity of produced $H_{2(g)}$ and $O_{2(g)}$

Gas purity is a valuable consideration as it is important that the gases produced from the electrolyser are pure, especially when the produced hydrogen gas is to be used to power a fuel cell. The PEM electrolyser was expected to provide high gas purity due to the low permeability of hydrogen and oxygen through the polymer electrolyte at SATP [4] [28]. PEM electrolysers are typically reported to produce hydrogen gas with a purity of 99.99%, and oxygen with a purity of 99% [45][46].

The thickness of the proton exchange membrane has an impact on the purity of the gases. A thin proton exchange membrane helps reduce resistance of ionic currents, but leads to an increase in gas permeation through the membrane. Since the thickness of the proton exchange membrane used for this work was very small, 45 μm, it is possible gas permeation may have occurred. Another aspect that may impact the purity of the gases is potential parasitic reactions, which are more significant at lower currents. The average ratio of measured $H_{2(g)}$ to $O_{2(g)}$for all 60 trials was measured to be 2.06 ± 0.03. As this ratio was very close to the expected ratio of 2, it was assumed that the gasses produced were indeed $H_{2(g)}$ and $O_{2(g)}$with high purities.

4.2 MJSC

Characteristic properties of the test MJSC were obtained through a series of experiments under practical operation conditions in order to determine its energy conversion efficiency. By first comparing the test MJSC to a reference cell system, a known relationship between solar concentration and the short circuit current of the test MJSC was quantified. Using that relationship, the light source was adjusted to a selection of practical solar concentrations, in the range of 0.5 Suns to 30 Suns. Such concentrations can easily be achieved using a Fresnel lens. Higher concentrations were not considered because the resulting currents were outside of the optimal operation range of the test PEM electrolyser, as established in the previous section. The *MPP* characteristic *I-U* and power-voltage curve of the test MJSC were obtained and analyzed to determine the *MPP* value at each solar concentration and the resulting energy conversion efficiency was calculated. All tests were performed at SATP and a TEC was used to maintain the temperature of the system.

4.2.1 Solar simulator calibration

The primary step to determining the energy conversion efficiency of the test MJSC was to obtain its 1 Sun short circuit current value, accomplished by use of a reference cell system. The reference cell system included a calibrated solar cell of which the 1 Sun short circuit current was known under an AM1.5 G filter. The reference solar cell used in this work considered the intensity of 1 Sun to be $1000\ \mathrm{W\,m^{-2}}$ and resultantly, that is the definition of 1 Sun used in this work as is the standard assumption for similar works. The reference solar cell was used to determine and effectively calibrate the total irradiance output of the solar simulator. Under a known intensity value, the short circuit current of the test MJSC was recorded and used as a reference to determine the short circuit current of other solar concentrations.

As the maximum irradiance output of the solar simulator with the AM1.5 G filter did not reach 1 Sun, the short circuit current of the test MJSC was measured under an irradiance of $500\ \mathrm{W\,m^{-2}}$,

or 0.5 Suns. The short circuit current for the 0.5 Suns measurement was then used to calculate the short circuit current for a 1 Sun measurement from the optical concentration relation:

$$I_{sc} = X\, I_{sc,1\ sun} \tag{22}$$

where X is the concentration ratio (in this case, 0.5) and $I_{SC,1\ sun}$ is the short circuit current at 1 Sun [47]. This relationship is only valid under uniform irradiance, constant temperature, and only within a moderate range of solar concentrations; this relationship is no longer valid at very high solar concentrations not studied in this report. As evident from the optical concentration relation, the short circuit current is linearly dependent on the total incident irradiance. A short circuit current under 1 Sun is twice the short circuit of the 0.5 Suns measurement. Five measurements of the *I-U* characteristics for the MJSC under 0.5 Suns illumination were performed and the measured short circuit currents were averaged to yield a value of $I_{sc} = 6.522 \times 10^{-3}$ A. From this value, a short circuit current under 1 Sun was determined to be $I_{sc} = 1.304 \times 10^{-2}$ A. Using this optical concentration ratio, the target short circuit currents for 0.5 Suns, 1 Sun, 5 Suns, 10 Suns, 15 Suns, 20 Suns, 25 Suns and 30 Suns were determined. The actual short circuit currents for each respective solar concentration based on the average of the five trials are displayed in a summary table at the end of this section, Table 4.2.1.

This method of scaling the input irradiance as a ratio of the solar cell's short circuit current is a commonly used standard approach [48]. Since the MJSC used was designed to operate under extremely high solar concentrations, up to 1000 Suns, and the operating range for the series of experiments was 0.5 Suns to 30 Suns, any series resistance within the MJSC is negligible at the studied solar concentrations [49]. The 1 Sun determination is necessary to obtain a reference for the input power for the MJSC and combined systems.

4.2.2 Characteristics of the MJSC

The characteristic properties of the test MJSC were evaluated under solar concentrations of 0.5 Suns to 30 Suns. The desired solar concentration was reached by adjusting the partial sun attenuator, which regulates the intensity output from the solar simulator until the short circuit current determined in section 4.2.1 and later presented in Table 4.2.1. was reached for each solar concentration. Once the desired concentration was reached and the temperature of the system equilibrated to 25 °C, a voltage sweep was performed. It was important to maintain the

temperature of the cell as the performance of the cell is dependent on temperature [50]. During the voltage sweep performed under constant illumination and temperature, the output current and applied voltage were measured at 0.01 V intervals. For each measurement, the corresponding voltage and current measurements were multiplied to obtain the power output of the MJSC at each studied voltage. The results are presented in Figure 4.2.1.

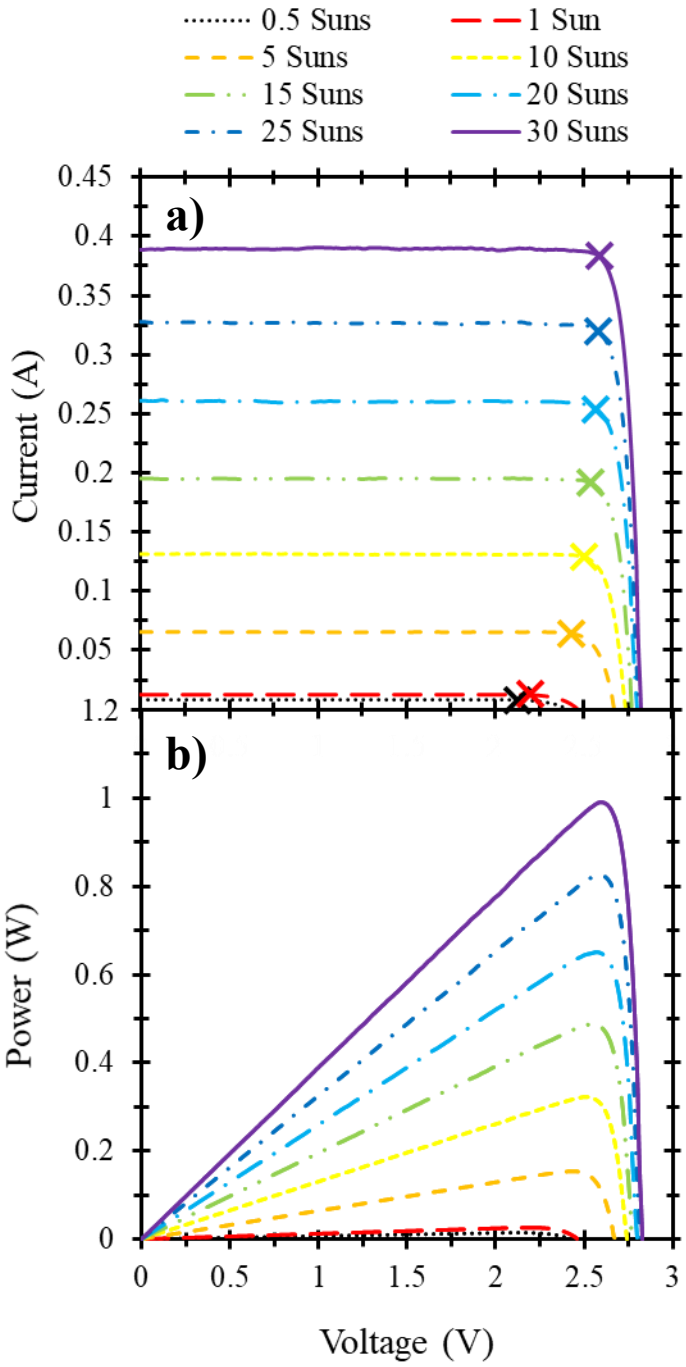

Figure 4.2.1: a) *I-U* curve and b) power-voltage curve of the test MJSC at SATP under various levels of illuminations. In chart a), the "X"'s for each trial's data indicates the location of the *MPP*.

Displayed in panel a) of Figure 4.2.1, the short circuit current, I_{sc} is found at voltages equal to zero and increases linearly with irradiance, as is by definition presented in equation (22). The open circuit voltage, found when the net current was zero, scales logarithmically with increasing irradiance. These results are to be expected under constant temperature and uniform irradiance at the concentrations studied.

The *MPP*, the point at which the product of the operating voltage and current is greatest, is indicated on panel a) by an "X" for each irradiance studied. To further demonstrate the power output of the test MJSC, the characteristic power-voltage curve of the test MJSC is presented in panel b). The *MPP* is at the peak of each of the power-voltage curves. The *MPP* increases with increasing irradiance. This observation was expected because as there is more light, a greater number of electrons are promoted to the conduction band from the valence band to generate a greater current at each of the studied voltages, for each irradiance trial. This increasing trend would gradually decrease as higher solar concentrations are reached as there will eventually be a limit to the current generated by the test MJSC. The *MPP* is later presented in Table 4.2.1.

To further evaluate the performance of the test MJSC, the fill factor was studied over the range of evaluated solar concentrations. The fill factor was 0.840 at 0.5 Suns, which increased to 0.869 at 1 Sun. The fill factor remained around 0.9 for the remaining evaluated solar concentrations. At low solar concentrations, the low current ultimately resulted in the lower fill factor as shunt parasitic resistances and side reactions had a greater overall impact on the current. At higher concentrations where there was a greater overall current, these factors had less of an impact. If higher solar concentrations were evaluated, the fill factor would be expected to drop as series resistance impacts the open circuit voltage [50]. Typical III-V MJSC have a fill factor in the mid to high eighties[51][52]. As the fill factor of the test MJSC under investigation was just at or under 0.9, it can be deduced that the cell was well crafted and operated effectively.

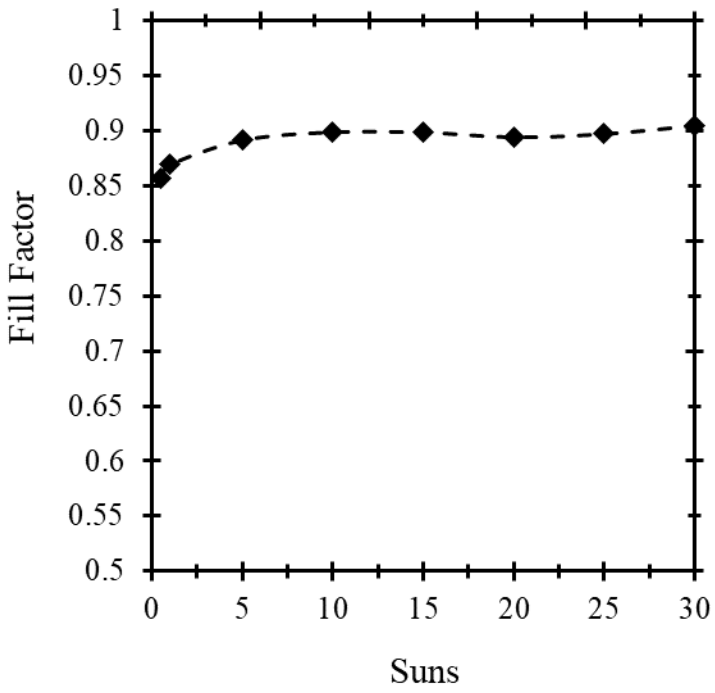

Figure 4.2.2: Fill factor of the test MJSC at SATP under varying solar concentrations.

The below table summarizes the characteristic properties of the test MJSC obtained in this section. In the previous section, the input current range which resulted in the PEM electrolyser having an efficiency greater than 90% was 60 mA to 440 mA. Solar concentrations less than 5 Suns and greater than 30 Suns would result in an output current that is outside of the ideal operating range of the PEM electrolyser.

Table 4.2.1: Characteristics of the MJSC summary

No. Suns	***Isc* (mA)**	***Uoc* (V)**	***MPP* (mW)**	**Fill Factor**
0.5	6.522	2.405	13.17	0.840
1	12.82	2.467	27.48	0.869
5	65.27	2.674	155.6	0.891
10	131.2	2.738	322.8	0.899
15	195.5	2.776	487.6	0.898
20	260.9	2.796	652	0.894
25	327.5	2.814	826.6	0.897
30	388.1	2.827	992	0.905

4.2.3 Efficiency of the MJSC

The energy conversion efficiency of the test MJSC was determined based on the measured power output. The efficiency was calculated for each of the studied solar concentrations using equation (16), which states:

$$\eta_{MJSC} = \frac{P_{out}}{P_{in}} \times 100\%$$

At the highest point of efficiency, the output power of the MJSC is the *MPP*:

$$P_{out} = MPP$$

The power input is the product of the intensity of 1 Sun, the solar concentration ratio at which the trial is conducted, and the area of the MJSC:

$$P_{in} = \Gamma_{1\,Sun} \mathrm{X}\, A_{MJSC}$$

A sample calculation of the efficiency of the trials conducted at 0.5 Suns is as follows:

$$MPP = 0.01317 \text{ W}$$

$$A_{MJSC} = 0.0001 \text{ m}^2$$

$$X = 0.5$$

$$\Gamma_{1\,Sun} = 1000 \text{ W m}^{-2}$$

$$\eta_{MJSC} = \frac{MPP}{P_{in} A_{MJSC}} \times 100 = 26.3\%$$

The energy conversion efficiency of the MJSC under a 0.5 Suns irradiance is 26.3%. The efficiency of the MJSC under the remaining solar concentrations is presented in Figure 4.2.3.

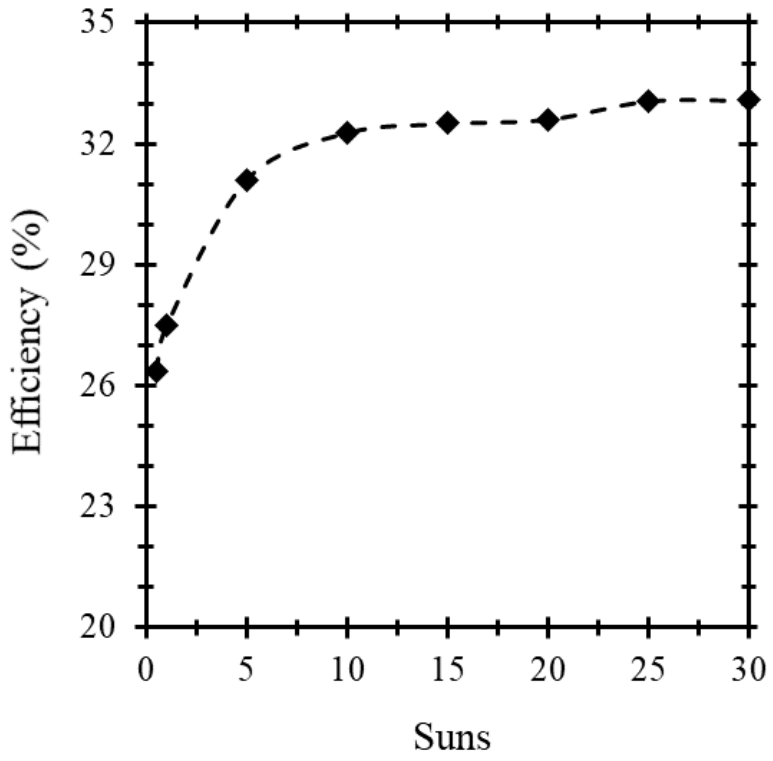

Figure 4.2.3: Efficiency of the test MJSC at SATP under varying solar concentrations.

The energy conversion efficiency of the MJSC under concentrated irradiance increased with solar concentration. Starting at 26.3% at 0.5 Suns, the efficiency only increased 1.2% between 0.5 Suns and 1 Sun. The greatest rate of change of efficiency occurred between 1 Sun and 5 Suns where the efficiency increased from 27.5 % to 31.1%. Between 5 Suns and 30 Suns, the efficiency gradually increased with solar concentration from 31.1% to 33.1%. This observed trend is in line with what is expected in this moderate range of solar concentrations. Under SATP a greater proportion of the incident is lost due to thermal emission as the solar cell attempts to achieve thermal equilibrium with its surroundings. This trend would not be expected to continue at very high solar concentrations when the series resistance would impede further efficiency improvements [50], for III-V MJSCs, this is expected to occur around 300 Suns [53].

The solar cell performance further indicates that the cell was well fabricated and the experimental set-up was well developed as the efficiency is in line with other current publications. Though it is difficult to directly compare any two systems as there are many

variables that will impact the efficiency of a MJSC including concentration, temperature, number of cell layers and composition of cell layer, MJSCs leading the industry in performance are typically reported to have efficiencies in the 30% under low concentrations, and 40% under high concentration [54].

As the efficiency is expected to increase until concentrations are reached that are ten times more intense than the ones evaluated in this work, it is evident that the evaluated solar concentrations do not result in an efficiency near the maximum efficiency of this solar cell. Despite the importance of maximizing the efficiency of the MJSC, greater solar concentrations were not considered as they would result in currents, which are outside of the optimal operation range of the PEM electrolyser.

4.3 Combined system

The STH energy conversion efficiency of the combined MJSC and PEM electrolyser system was measured under varying solar concentrations and the optimal operation conditions were identified. The PEM electrolyser was first analyzed separately to determine the range of input currents, which resulted in an efficiency of 90% or greater. As the MJSC was used to power the PEM electrolyser, the optimal input current range of the PEM electrolyser translated to the target output current of the MJSC. Characteristic properties and the energy conversion efficiency of the MJSC were then measured under a range of solar concentrations, which resulted in the target output currents. The overall energy conversion efficiency of the combined system is the product of the efficiency of the PEM electrolyser and the MJSC separately, while operating in tandem as presented in equation (19).

4.3.1 Efficiency of the PEM electrolyser with power supplied by the MJSC

The performance of the PEM electrolyser when in the combined system was evaluated to determine if the different power source impacts the efficiency, as well as to contribute to the eventual determination of the overall STH efficiency. In order to calculate the energy conversion efficiency of the PEM electrolyser in the combined set-up, the timeframe required to produce 27.5 mL of hydrogen was calculated using equation (21) based on the output current of the MJSC at the test solar concentrations and the load introduced by the PEM electrolyser. To accomplish this, the current at the leads to the PEM electrolyser was measured when connected to the MJSC at the test solar concentration after the electrolyser had time to accumulate charge. Using the previously determined *I-U* characteristics of the PEM electrolyser, the voltage introduced by the PEM electrolyser was estimated. This was an important measurement as the known short circuit current could not have been used as the output current of the MJSC varied with load. Furthermore, the voltage of the PEM electrolyser could not be assumed based on the short circuit current of the MJSC because the potential difference across the cell varied based on input current. The measured input current to the PEM electrolyser and the estimated potential difference for each solar concentration is presented later in Table 4.3.1.

Once the experimental time for each solar concentration was determined and the trials were performed, the energy conversion efficiency of the PEM electrolyser was calculated using

equation (15). The overall energy conversion efficiency, as well as the Faraday and voltage efficiencies, of the PEM electrolyser when powered by the MJSC is presented in Figure 4.3.1.

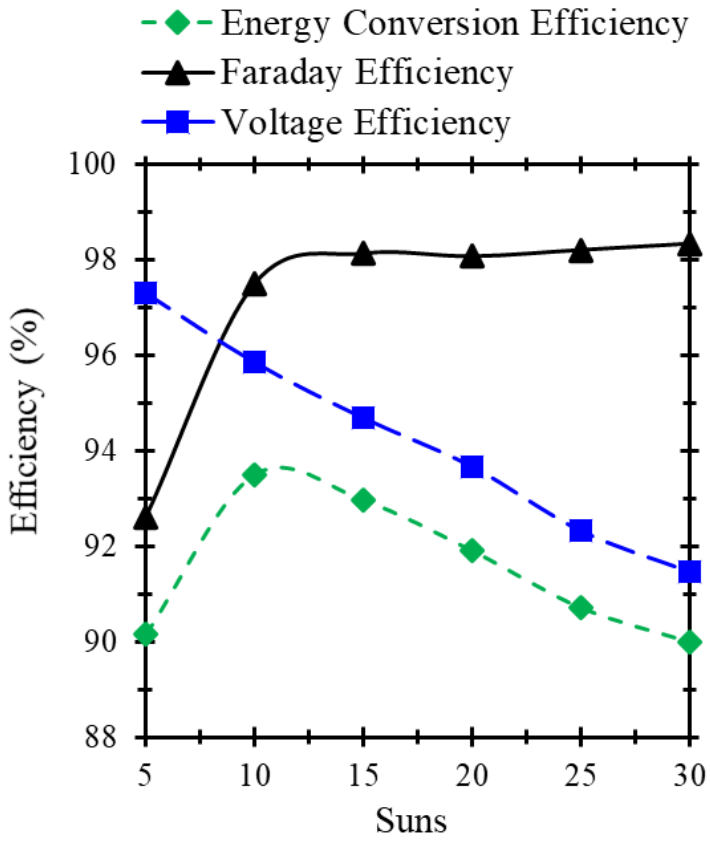

Figure 4.3.1: Efficiency of the PEM electrolyser when powdered by the MJSC.

For all of the solar concentrations evaluated, the energy conversion efficiency of the PEM electrolyser was measured to be greater than 90%. There was a large increase in efficiency between 5 Suns and 10 Suns where the PEM electrolyser achieved its greatest efficiency of 93.7%. Between 10 Suns and 30 Suns, the efficiency of PEM electrolyser steadily decreased. The efficiency's response to solar concentration may be described by the individual Faraday and voltage efficiencies. At 5 Suns, the Faraday efficiency was limiting, which indicates that not all of the input current was used for the dissociation reaction from water to hydrogen and oxygen gas. Between 5 Suns and 10 Suns, the Faraday and voltages efficiencies crossed so that the voltage efficiency became limiting. This indicates that the potential difference greater than the thermoneutral voltage of 1.481 V was the limiting factor for the 10 Suns to 30 Suns trials. The shape and values of the efficiency of the PEM electrolyser in response to the varying solar

concentrations is aligned with the complimentary efficiency graph of the isolated PEM electrolyser presented in Figure 4.1.3. As the input current was measured for each of the solar concentrations, the performance of the PEM electrolyser when powered by the MJSC may easily be compared to the isolated system. The isolated system resulted in an efficiency greater than 90% for the input current range 60 mA to 440 mA. When powered by the MJSC, the PEM electrolyser was measured to have a comparable efficiency; the efficiency was greater than 90% between the input current range 65.27 mA to 388.1 mA. The highest efficiency of the isolated system was achieved at an input current of 180 mA. When powered by the MJSC, the greatest measured efficiency was achieved at an input current of 131.2 mA. The difference between the currents resulting in the greatest efficiency of the isolated and combined PEM electrolyser trials is likely a result of the granularity of the measurements for the combined system. When evaluating the isolated system, trials were performed at an interval of 20 mA, while the combined system was measured in 65 mA intervals. The details for each of the trials and the determined efficiencies are summarized in Table 4.3.1. Overall, the performance of the PEM electrolyser when isolated and powered by the MJSC were in agreement indicating that the MJSC did not impact the efficiency of the PEM electrolyser.

Table 4.3.1: Summary of PEM electrolyser efficiency when powered by the MJSC

No. Suns	I_{OP} (mA)	V_{OP} (V)	Time (s)	Faraday Efficiency (%)	Voltage Efficiency (%)	Energy Conversion Efficiency (%)
5	65.27	1.517	3322	92.6	97.6	90.5
10	131.2	1.541	1662	97.5	96.1	93.7
15	195.5	1.562	1108	98.1	94.8	93.1
20	260.9	1.581	831	98.1	93.7	91.9
25	327.5	1.600	661	98.2	92.6	91.0
30	388.1	1.616	557	98.3	91.7	90.2

4.3.2 Efficiency of the MJSC when powering the PEM electrolyser

The efficiency of the MJSC when supplying power to the PEM electrolyser was evaluated. Unlike the PEM electrolyser, the MJSC in the combined system was not expected to have a similar performance to the separate MJSC. The experimental set up of the combined system ensured that the output current of the MJSC was in the ideal operating range for the PEM electrolyser. At that input current, the PEM electrolyser introduced a load on the system, which was not tunable. Resultantly, the potential difference across the MJSC and the operating current

for the combined system trials did not align with the characteristic *MPP* of the MJSC. The *I-U* characteristics of the separate MJSC and PEM electrolyser are overlaid and presented in Figure 4.3.2.

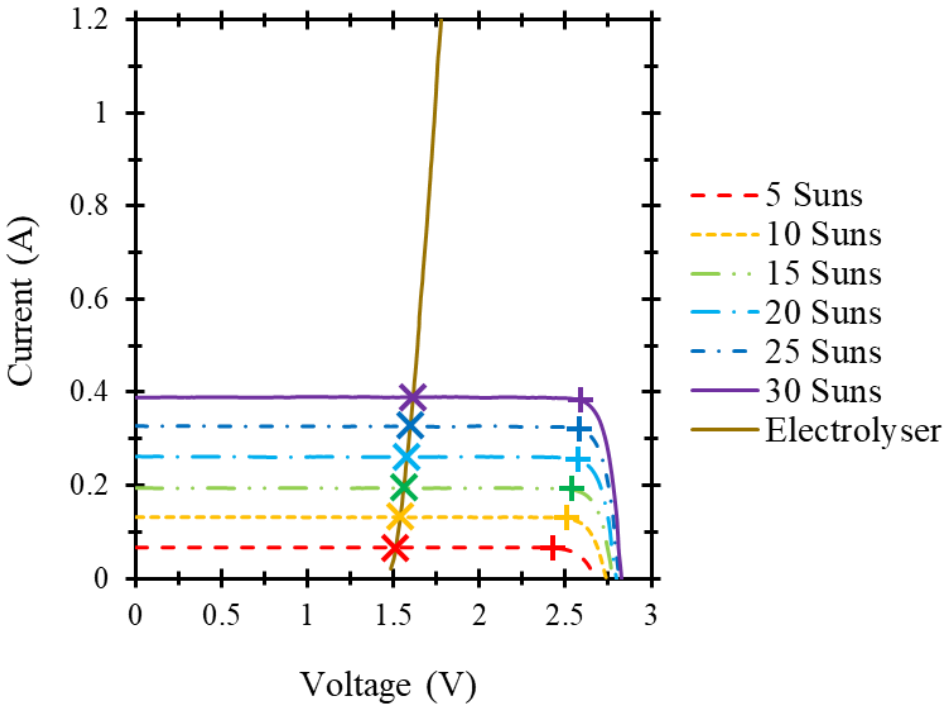

Figure 4.3.2: *I-U* curve of the PEM electrolyser and the test MJSC under various levels of illuminations at SATP. The "X"'s indicate the location of the combined system's operating power point and the "+"'s indicate the *MPP* of the MJSC.

From Figure 4.3.2 it can be seen that the operating power point of the combined system was not at, or very near, the *MPP* of the MJSC. The further the operating power point is from the *MPP* of the MJSC, the lower the expected efficiency of the MJSC in the combined system.

The efficiency of the MJSC when in the combined system was calculated using equation (16) and the results are presented in Figure 4.3.3. In the same figure, the efficiency of the MJSC when

operating at the *MPP* is also presented to demonstrate the reduction in efficiency as a result of not operating at the *MPP*.

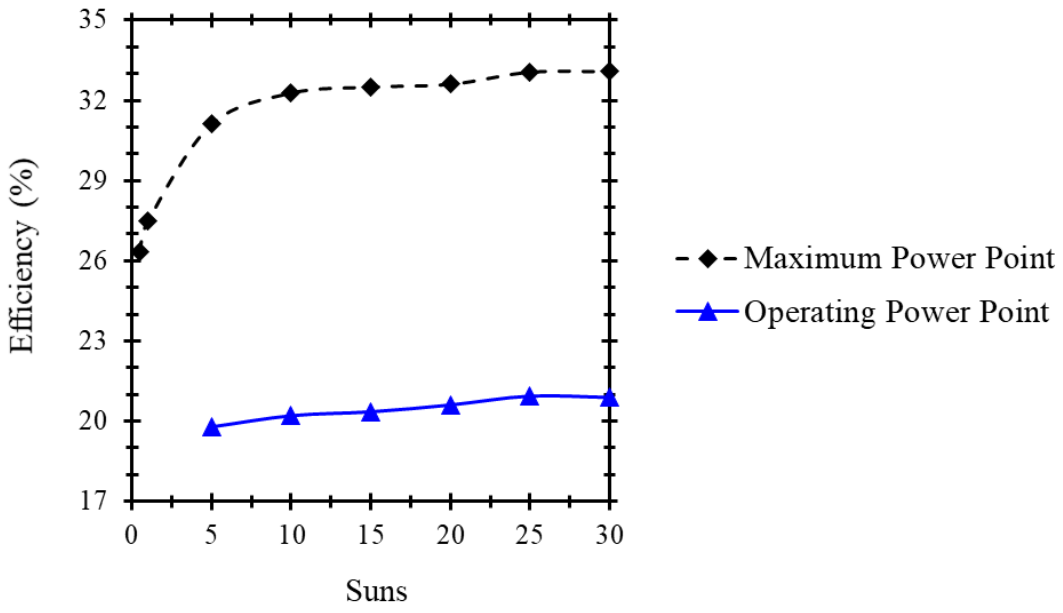

Figure 4.3.3: The efficiency of the MJSC at varying solar concentrations at the *MPP* of the MJSC, and the efficiency of the MJSC operating at the voltage produced by the electrolyser, the operating power point

The combined system trials began at a solar concentration of 5 Suns. The efficiency of the MJSC in the combined system was 19.8%. The efficiency increased to 20.2% at 10 Suns, and remained below 21% for the remaining solar concentrations. These efficiencies are well below the efficiency of the cell when operating at the *MPP*. Furthermore, the relationship of the efficiencies between the combined system and isolated system at a given solar concentration is not constant between solar concentrations. This observation may be explained by considering how the relationship between the *MPP* and the operating power point presented in Figure 4.3.2 is not linear.

4.3.3 Overall Energy Conversion Efficiency

The overall STH energy conversion efficiency of the one-to-one MJSC to PEM electrolyser system under varying solar concentrations was evaluated using equation (19) based on the measured efficiencies of each system while in combination. The STH efficiency was evaluated for varying solar concentrations, which resulted in output currents from the MJSC in the ideal

operating range for the PEM electrolyser. Unlike the electrolyser and as made evident by Figure 4.3.2, the MJSC was not operating near its maximum efficiency. Preparing a combined system in which both the MJSC and PEM electrolyser operate at their maximal efficiency could be achieved by having multiples of each system connected in series and/or parallel, by using an electronic converter, or *MPP* tracker. This is discussed in more detail in section 5.2. As a system accounting for operating efficiency is achievable, the theorized maximum of the combined system was determined by assuming the MJSC is operating at the maximum power point of the isolated system. Both the actual STH efficiency and the theorized maximum STH efficiency are presented in Figure 4.3.4.

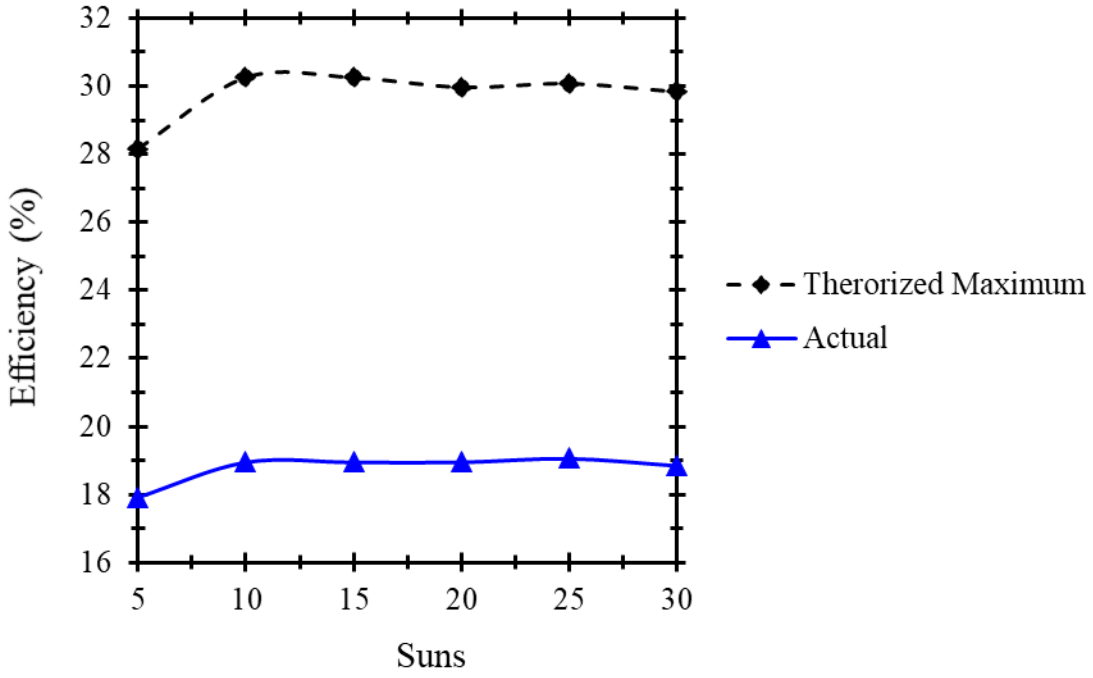

Figure 4.3.4: STH efficiency of the combined PEM electrolyser and MJSC system.

For the actual STH efficiency of the one-to-one system, the efficiency was measured to be 17.9% for a solar concentration of 5 Suns, and 19.0% for 10 Suns to 20 Suns, 19.1% for 25 Suns, and 18.9% for 30 Suns. The maximum theorized efficiency of the combined system was calculated to

be at most 30.3% at 10 Suns and 15 Suns, this corresponds to the solar concentrations that resulted in the most efficient operation of the PEM electrolyser.

The actual performance of the system without system optimization is superior to systems, which employ silicon SJSC and do consider system optimization. As typical silicon SJSC operate at voltages below the thermoneutral voltage to split water, a one-to-one system is not possible. In a three-to-one silicon SJSC electrolyser system, a STH energy conversion efficiency of 14% has been reported [55]. The silicon SJSC PEM electrolyser system was lower in efficiency relative to the system presently under investigation because of the comparatively low efficiency of the solar cell, which was measured to be 20.6%.

This combined system used a commercially available MJSC and PEM electrolyser. The MJSC and PEM electrolysers had typical performances relative to similar, modern devices. In the practical work of Nakamura et al. from 2015., the STH efficiency was measured for a MJSC under concentration and PEM electrolyser system [32]. The PEM electrolyser and MJSC were both very similar to the ones presently under investigation. They studied different system configurations to determine, which ratio of solar cells and electrolyser systems resulted in the greatest efficiency. The greatest STH efficiency that they achieved was 24.4% when the system was composed of 5 electrolysers and 3 solar cells. The efficiency of the MJSC varied based on the configuration, but the efficiency for the configuration, which resulted in the maximum efficiency was 31.2% under approximately 22 Suns. The efficiency of the PEM electrolyser was measured to be 71.1% in this configuration by considering 1.23 V to be the minimum voltage required to drive the electrolysis reaction. If the thermoneutral voltage of 1.48 V was used, the PEM electrolyser energy conversion efficiency would be 85.6% and the overall STH efficiency would be 29.1%. These values are slightly lower than the theorized maximum STH efficiency value estimated in this work if system configuration optimization was achieved, but it is higher than the actual value obtained without system configuration optimization. The work of Nakamura et al. demonstrates that not only optimizing the system configuration is possible and can practically increase the STH efficiency, but it also demonstrates that practical systems are achievable and will reach efficiencies close to those theorized.

5 Conclusions

5.1 Summary

The STH energy conversion efficiency of a one-to-one MJSC PEM electrolyser system was evaluated. The isolated systems were first evaluated to determine the operation conditions, which resulted in the greatest efficiency of the respective systems at SATP. The PEM electrolyser achieved an efficiency greater than 90% when the input current was in the range of 60 mA to 440 mA. At each of the evaluated solar concentrations, the current and voltage of the *MPP* were determined for the MJSC. The efficiency of the MJSC was measured at the *MPP* for each of the solar concentrations evaluated. The efficiency increased with increasing solar concentration and was at most 33.1% at 30 Suns.

When evaluating the combined system, the output current of the MJSC at the *MPP* did not fall within the range of the optimal operation conditions of the PEM electrolyser. The combined system trials were performed so that the output current of the MJSC was in the ideal range for the PEM electrolyser and as such, the MJSC did not operate at its *MPP*. The overall STH energy conversion efficiency of the system was measured to be at most 19.1% under 25 Suns. If the MJSC was operating at its *MPP*, then the overall STH energy conversion efficiency is theorized to be 30.3% at 10 Suns to 15 Suns.

5.2 Future work

This work focused on measuring the STH efficiency of a one-to-one PEM electrolyser and MJSC system. This fundamental research will provide the base information to those seeking to understand and model PEM electrolyser and MJSC systems. This work can be developed in the future by considering optimal system configurations, which is an important aspect of practical systems. The scope of this work only considered a one-to-one system and, in this system, the maximum operating voltage and current conditions for the individual systems did not align. By considering optimal system configurations, the efficiency would be improved. As these systems

are expensive, it is practical to ensure that they are operating at or near their maximum efficiencies.

Optimal system configurations may be achieved by connecting multiple PEM electrolyser and MJSC in series and/or parallel. The following equations describe the current (I_{total}) and voltage (U_{total}) across n modules connected in parallel

$$I_{total} = \sum I_n \tag{23}$$

$$U_{total} = U_n = U_{n+1} = U_{n+2} \dots \tag{24}$$

As shown in equation (23) the total current across a number of cells connected in parallel is the sum of the current across each cell. Since the cells connected in parallel share equivalent voltages, the total voltage across a number of cells connected in parallel is equivalent to the voltage across each cell as displayed in equation (24). Alternatively, the following equations describe the current and voltage across n cells in series

$$U_{total} = \sum U_n \tag{25}$$

$$I_{total} = I_n = I_{n+1} = I_{n+2} \dots \tag{26}$$

As shown in equation (25) the total voltage across a number of cells connected in series is the sum of the voltage across each cell. Since the cells connected in series share equivalent currents, the total current across a number of cells connected in series is equivalent to the current across each cell as displayed in equation (26). By considering the optimal voltage and current values, which result in the greatest efficiency for both the PEM electrolyser and the MJSC, as

determined in the thesis, the optimal system configuration can be determined from the following equations

$$\frac{U_{PEM}}{U_{MPP}} = R_s \tag{27}$$

$$\frac{I_{PEM}}{I_{MPP}} = R_p \tag{28}$$

Where U_{PEM} and I_{PEM} are the optimal voltage and current respectively for the PEM electrolyser and U_{MPP} and I_{MPP} are the optimal voltage and current respectively of for MJSC. Equation (27) determines the ratio of PEM electrolysers to MJSCs connected in series, whereas equation (28) determines the ratio of PEM electrolysers to MJSCs connected in parallel represented by R_s and R_p respectively.

When multiples of each system are not available, an *MPP* tracking system with boost converters may also be used to result in a system in which both devices are operating at the ideal current and voltages. *MPP* tracking system boost converters work through the constant adjustment of the operating voltage across the MJSC by applying varying resistance across the cell. *MPP* tracking systems are typically used on concentrated photovoltaics to respond to fluctuations in insolation. Since the bottle neck in the STH efficiency is the MJSC efficiency, employing an *MPP* tracking system is an ideal method to ensure high operating efficiency of the MJSC system. Recently, a method of *MPP* tracking was proposed and was able to ensure that the solar cell was operating at its *MPP* with an efficiency of approximately 100% [56].

A final method to ensure that the systems are both operating under the ideal conditions is through the employment of a switch-mode DC-voltage regulator. A switch-mode DC-voltage regulator may be used to regulate the input current or voltage to the PEM electrolyser system to ensure that the PEM electrolyser is working under the most efficient conditions [57]. A comparison and analysis of the methods used to ensure that the maximum efficiency is reached was recently performed [58].

6 Appendices

6.1 Uncertainty of measurements

All reported values only include one uncertain digit. Uncertainty of any measured value Z was measured by the following equation:

$$\Delta Z = [\Delta A^2 + \Delta B^2]^{1/2} \quad (29)$$

Where ΔA is the standard error of the mean of Z and ΔB is the uncertainty introduced by the instruments used to obtain Z [59].

All instruments used to obtain any measured value in this work are presented in the Table 6.1.1: Measurement accuracy of instruments with their associated accuracy.

Table 6.1.1: Measurement accuracy of instruments

Instrument	Measurement Type	Range	Accuracy
Keithley 2420 SMU	Source voltage	(0 - 0.2 V]	0.02% + 0.0006 V
		(0.2 - 2 V]	0.02% + 0.0006 V
		(2 - 20 V]	0.02% + 0.024 V
	Measured voltage	(0.2 - 2 V]	0.012% + 0.0003 V
	Source current	(0 - 0.1 A]	0.066% + 0.00002 A
		(0.1 - 1 A]	0.067% + 0.0009 A
		(1 - 3 A]	0.059% + 0.0027 A
	Measured current	(0 - 0.01 A)	0.035% + 0.0000006 A
		(0.01 - 0.1 A)	0.055% + 0.000006 A
		(0.1 - 1 A)	0.066% + 0.00057 A
PEM electrolyser	Gas Volume	[0 - 30 mL]	0.25 mL

6.2 PEM electrolyser results summary

Table 6.2.1: Summary of PEM electrolyser Results

Current (A)	Average Voltage (V)	Time (s)	Faraday Efficiency (%)	Voltage Efficiency (%)	Energy Conversion Efficiency (%)	H2:O2
0.020	1.487	10800	78	99.6	77.2	2.07
0.040	1.503	5400	87	98.5	85.4	2.11
0.060	1.515	3600	92.0	97.8	90.0	2.08
0.080	1.522	2700	93.0	97.3	90.5	2.08
0.100	1.530	2160	94.8	96.8	91.8	2.04
0.120	1.539	1800	96	96.3	91.3	2.04
0.140	1.545	1543	95.7	95.9	91.8	2.02
0.160	1.552	1350	96.6	95.4	92.2	2.04
0.180	1.557	1200	98.4	95.1	93.7	2.08
0.200	1.564	1080	98.4	94.7	93.2	2.08
0.220	1.570	982	98.4	94.3	92.9	2.08
0.240	1.574	900	98.4	94.1	92.7	2.08
0.260	1.581	831	98.4	93.7	92.2	2.08
0.280	1.587	771	98.5	93.3	91.9	2.08
0.300	1.592	720	98.4	93.0	91.6	2.00
0.320	1.597	675	98.4	92.7	91.3	2.00
0.340	1.604	635	98.5	92.3	91.0	2.08
0.360	1.609	600	98.4	92.1	90.7	2.00
0.380	1.614	568	98.5	91.8	90.5	2.00
0.400	1.619	540	98.4	91.5	90.1	2.08
0.420	1.623	514	98.5	91.3	89.9	2.00
0.440	1.628	491	98.4	91.0	89.6	2.00
0.460	1.633	470	98.3	90.7	89.2	2.00
0.480	1.638	450	98.4	90.4	89.1	2.00
0.500	1.642	432	98.4	90.2	88.8	2.00
0.520	1.645	415	98.5	90.0	88.7	2.04
0.540	1.650	400	98.4	89.8	88.4	2.08
0.560	1.652	386	98.4	89.6	88.2	2.08
0.580	1.656	372	98.5	89.4	88.2	2.08
0.600	1.660	360	98.4	89.2	87.9	2.08
0.620	1.665	348	98.5	89.0	87.7	2.08
0.640	1.670	338	98.3	88.7	87.2	2.08
0.660	1.674	327	98.5	88.5	87.2	2.08
0.680	1.678	318	98.3	88.3	86.8	2.08
0.700	1.683	309	98.3	88.0	86.6	2.08
0.720	1.687	300	98.4	87.8	86.4	2.08

0.740	1.692	292	98.4	87.6	86.2	2.08
0.760	1.696	284	98.5	87.3	86.1	2.08
0.780	1.700	277	98.4	87.1	85.8	2.08
0.800	1.703	270	98.4	87.0	85.6	2.08
0.820	1.708	263	98.6	86.7	85.5	2.08
0.840	1.711	257	98.5	86.6	85.3	2.08
0.860	1.716	251	98.5	86.3	85.1	2.08
0.880	1.718	245	98.6	86.2	85.0	2.08
0.900	1.723	241	98.0	86.0	84.3	2.08
0.920	1.727	235	98.3	85.8	84.4	2.08
0.940	1.730	230	98.3	85.6	84.2	2.08
0.960	1.734	225	98.4	85.4	84.1	2.08
0.980	1.738	220	98.6	85.2	84.1	2.08
1.000	1.742	216	98.4	85.0	83.7	2.08
1.020	1.745	212	98.3	84.9	83.5	2.08
1.040	1.748	208	98.3	84.7	83.3	2.08
1.060	1.751	204	98.3	84.6	83.2	2.08
1.080	1.754	200	98.4	84.4	83.1	2.08
1.100	1.757	196	98.6	84.3	83.2	2.08
1.120	1.761	193	98.4	84.1	82.8	2.08
1.140	1.766	189	98.7	83.9	82.8	2.08
1.160	1.770	186	98.5	83.7	82.5	2.08
1.180	1.775	183	98.5	83.5	82.2	2.08
1.200	1.779	180	98.4	83.3	82.0	2.08

6.3 References

[1] K. Fujii, S. Nakamura, M. Sugiyama, K. Watanabe, B. Bagheri, and Y. Nakano, "Characteristics of hydrogen generation from water splitting by polymer electrolyte electrochemical cell directly connected with concentrated photovoltaic cell," *Int. J. Hydrogen Energy*, vol. 38, no. 34, pp. 14424–14432, 2013.

[2] Ontario Energy Board and Government of Ontario, "Ontario Energy Report Q4 2018," 2018.

[3] P. P. Edwards, V. L. Kuznetsov, W. I. F. David, and N. P. Brandon, "Hydrogen and fuel cells: towards a sustainable energy future," *Energy Policy*, vol. 36, no. 12, pp. 4356–4362, 2008.

[4] M. Carmo, D. L. Fritz, J. Mergel, and D. Stolten, "A comprehensive review on PEM water electrolysis," *Int. J. Hydrogen Energy*, vol. 38, no. 12, pp. 4901–4934, 2013.

[5] K. Mazloomi and C. Gomes, "Hydrogen as an energy carrier: Prospects and challenges," *Renew. Sustain. Energy Rev.*, vol. 16, no. 5, pp. 3024–3033, 2012.

[6] S. Verhelst and T. Wallner, "Hydrogen-fueled internal combustion engines," *Prog. Energy Combust. Sci.*, vol. 35, no. 6, pp. 490–527, 2009.

[7] M. Balat, "Potential importance of hydrogen as a future solution to environmental and transportation problems," *Int. J. Hydrogen Energy*, vol. 33, no. 15, pp. 4013–4029, 2008.

[8] K. W. Harrison, R. Remick, A. Hoskin, and G. D. Martin, "Hydrogen production: fundamentals and case study summaries," National Renewable Energy Lab.(NREL), Golden, CO (United States), 2010.

[9] D. Bessarabov, H. Wang, H. Li, and N. Zhao, *PEM electrolysis for hydrogen production: principles and applications*. CRC press, 2016.

[10] A. Godula-Jopek, *Hydrogen production: by electrolysis*. John Wiley & Sons, 2015.

[11] M. Sarno and E. Ponticorvo, "High hydrogen production rate on RuS2@ MoS2 hybrid nanocatalyst by PEM electrolysis," *Int. J. Hydrogen Energy*, vol. 44, no. 9, pp. 4398–4405, 2019.

[12] B. Paul and J. Andrews, "Optimal coupling of PV arrays to PEM electrolysers in solar-hydrogen systems for remote area power supply," *Int. J. Hydrogen Energy*, vol. 33, no. 2, pp. 490–498, 2008.

[13] J. Nelson, *The physics of solar cells*. London: Imperial College Press, 2002.

[14] M. A. Green, E. D. Dunlop, D. H. Levi, J. Hohl-Ebinger, M. Yoshita, and A. W. Y. Ho-Baillie, "Solar cell efficiency tables (version 54)," *Prog. Photovoltaics Res. Appl.*, vol. 27, no. 7, pp. 565–575, 2019.

[15] A. Luque and S. Hegedus, *Handbook of photovoltaic science and engineering*. John Wiley

& Sons, 2011.

[16] A. Jäger-Waldau, “Status and perspectives of thin film photovoltaics,” *Thin Film Solar Cells: Current Status and Future Trends*. Nova Publishers, New York, NY, USA, pp. 1–24, 2010.

[17] L. C. Andreani, A. Bozzola, P. Kowalczewski, M. Liscidini, and L. Redorici, “Silicon solar cells: Toward the efficiency limits,” *Adv. Phys. X*, vol. 4, no. 1, p. 1548305, 2019.

[18] N. Jain and M. K. Hudait, “III–V multijunction solar cell integration with silicon: Present status, challenges and future outlook,” *Energy Harvest. Syst.*, vol. 1, no. 3–4, pp. 121–145, 2014.

[19] K. Yoshikawa *et al.*, “Silicon heterojunction solar cell with interdigitated back contacts for a photoconversion efficiency over 26%,” *Nat. Energy*, vol. 2, no. 5, p. 17032, 2017.

[20] W. Shockley and H. J. Queisser, “Detailed balance limit of efficiency of p-n junction solar cells,” *J. Appl. Phys.*, vol. 32, no. 3, pp. 510–519, 1961.

[21] S. Kurtz and D. Levi, “Conversion efficiencies of best research solar cells worldwide from 1976 through 2017 for various photovoltaic technologies,” *Natl. Renew. Energy Lab.*, 2017.

[22] T. J. McMahon, T. S. Basso, and S. R. Rummel, “Cell shunt resistance and photovoltaic module performance,” in *Conference Record of the Twenty Fifth IEEE Photovoltaic Specialists Conference-1996*, 1996, pp. 1291–1294.

[23] P. Singh and N. M. Ravindra, “Temperature dependence of solar cell performance—an analysis,” *Sol. Energy Mater. Sol. Cells*, vol. 101, pp. 36–45, 2012.

[24] C. A. Gueymard, D. Myers, and K. Emery, “Proposed reference irradiance spectra for solar energy systems testing,” *Sol. Energy*, vol. 73, no. 6, pp. 443–467, 2002.

[25] Y. A. Eltbaakh, M. H. Ruslan, M. A. Alghoul, M. Y. Othman, K. Sopian, and M. I. Fadhel, “Measurement of total and spectral solar irradiance: Overview of existing research,” *Renew. Sustain. Energy Rev.*, vol. 15, no. 3, pp. 1403–1426, 2011.

[26] ASTM, “G173-03 Reference Spectra Derived from SMARTS v. 2.9. 2 (AM1. 5), American Society for Testing and Materials.” 2011.

[27] ASTM, “490. 2000 American Society for Testing & Materials (ASTM) standard extraterrestrial solar spec-trum reference E-490-00 (2000),” *Recuper. http//rredc. nrel. gov/solar/spectra/am0*.

[28] F. Barbir, “PEM electrolysis for production of hydrogen from renewable energy sources,” *Sol. Energy*, vol. 78, no. 5, pp. 661–669, 2005.

[29] S. Licht, “Solar water splitting to generate hydrogen fuel: photothermal electrochemical analysis,” *J. Phys. Chem. B*, vol. 107, no. 18, pp. 4253–4260, 2003.

[30] O. Khaselev and J. A. Turner, “A monolithic photovoltaic-photoelectrochemical device for hydrogen production via water splitting,” *Science (80-.).*, vol. 280, no. 5362, pp. 425–

427, 1998.

[31] F. Dimroth, G. Peharz, U. Wittstadt, B. Hacker, and A. W. Bett, “Hydrogen production in a PV concentrator using III-V multi-junction solar cells,” in *2006 IEEE 4th World Conference on Photovoltaic Energy Conference*, 2006, vol. 1, pp. 640–643.

[32] A. Nakamura *et al.*, “A 24.4% solar to hydrogen energy conversion efficiency by combining concentrator photovoltaic modules and electrochemical cells,” *Appl. Phys. Express*, vol. 8, no. 10, 2015.

[33] J. Jia *et al.*, “Solar water splitting by photovoltaic-electrolysis with a solar-to-hydrogen efficiency over 30%,” *Nat. Commun.*, vol. 7, no. May, pp. 1–6, 2016.

[34] S. Rau *et al.*, “Highly efficient solar hydrogen generation—an integrated concept joining III–V solar cells with PEM electrolysis cells,” *Energy Technol.*, vol. 2, no. 1, pp. 43–53, 2014.

[35] J. J. Wysocki and P. Rappaport, “Effect of temperature on photovoltaic solar energy conversion,” *J. Appl. Phys.*, vol. 31, no. 3, pp. 571–578, 1960.

[36] L. E. Bell, “Cooling, heating, generating power, and recovering waste heat with thermoelectric systems,” *Science (80-.).*, vol. 321, no. 5895, pp. 1457–1461, 2008.

[37] M. Matus, “Temperature measurement in dimensional metrology–why the Steinhart-Hart equation works so well,” *Proc. MacroScale 2011*, 2011.

[38] M. M. Mench, *Fuel Cell Engines*. John Wiley & Sons, 2008.

[39] A. Fallisch *et al.*, “Investigation on PEM water electrolysis cell design and components for a HyCon solar hydrogen generator,” *Int. J. Hydrogen Energy*, vol. 42, no. 19, pp. 13544–13553, 2017.

[40] P. Millet, N. Mbemba, S. A. Grigoriev, V. N. Fateev, A. Aukauloo, and C. Etiévant, “Electrochemical performances of PEM water electrolysis cells and perspectives,” *Int. J. Hydrogen Energy*, vol. 36, no. 6, pp. 4134–4142, 2011.

[41] K. E. Ayers *et al.*, “Research advances towards low cost, high efficiency PEM electrolysis,” *ECS Trans.*, vol. 33, no. 1, pp. 3–15, 2010.

[42] S. A. Grigoriev *et al.*, “Hydrogen safety aspects related to high-pressure polymer electrolyte membrane water electrolysis,” *Int. J. Hydrogen Energy*, vol. 34, no. 14, pp. 5986–5991, 2009.

[43] H. A. Khater, A. A. Abdelraouf, and M. H. Beshr, “Optimum alkaline electrolyzer-proton exchange membrane fuel cell coupling in a residential solar stand-alone power system,” *ISRN Renew. Energy*, vol. 2011, 2011.

[44] R. García-Valverde, N. Espinosa, and A. Urbina, “Simple PEM water electrolyser model and experimental validation,” *Int. J. Hydrogen Energy*, vol. 37, no. 2, pp. 1927–1938, 2012.

[45] C.-C. Sung and C.-Y. Liu, “A novel micro protective layer applied on a simplified PEM

water electrolyser," *Int. J. Hydrogen Energy*, vol. 38, no. 24, pp. 10063–10067, 2013.

[46] R. Balaji *et al.*, "Development and performance evaluation of Proton Exchange Membrane (PEM) based hydrogen generator for portable applications," *Int. J. Hydrogen Energy*, vol. 36, no. 2, pp. 1399–1403, 2011.

[47] P. Pérez-Higueras and E. F. Fernández, *High concentrator photovoltaics: fundamentals, engineering and power plants*. Springer, 2015.

[48] C. R. Osterwald, "Translation of device performance measurements to reference conditions," *Sol. Cells*, vol. 18, no. 3–4, pp. 269–279, 1986.

[49] J. Zeitouny, E. A. Katz, A. Dollet, and A. Vossier, "Band gap engineering of multi-junction solar cells: Effects of series resistances and solar concentration," *Sci. Rep.*, vol. 7, no. 1, p. 1766, 2017.

[50] G. S. Kinsey, P. Hebert, K. E. Barbour, D. D. Krut, H. L. Cotal, and R. A. Sherif, "Concentrator multijunction solar cell characteristics under variable intensity and temperature," *Prog. Photovoltaics Res. Appl.*, vol. 16, no. 6, pp. 503–508, 2008.

[51] H. Cotal *et al.*, "III–V multijunction solar cells for concentrating photovoltaics," *Energy Environ. Sci.*, vol. 2, no. 2, pp. 174–192, 2009.

[52] E. Veinberg-Vidal *et al.*, "Manufacturing and characterization of III-V on silicon multijunction solar cells," *Energy Procedia*, vol. 92, pp. 242–247, 2016.

[53] C. R. Osterwald, M. W. Wanlass, T. Moriarty, M. A. Steiner, and K. A. Emery, "Effects of spectral error in efficiency measurements of GaInAs-based concentrator solar cells," National Renewable Energy Lab.(NREL), Golden, CO (United States), 2014.

[54] K. Ali, A. Khalid, M. R. Ahmad, H. M. Khan, I. Ali, and S. K. Sharma, "Multi-junction (III–V) solar cells: From basics to advanced materials choices," in *Solar Cells*, Springer, 2020, pp. 325–350.

[55] A. H. A. Rahim, A. S. Tijani, M. Fadhlullah, S. Hanapi, and K. I. Sainan, *Optimization of direct coupling solar PV panel and advanced alkaline electrolyzer system*, vol. 79. Elsevier B.V., 2015.

[56] M. Ashraf, "Analytical solutions for high efficiency maximum power point tracking boost converters," *Int. J. Circuit Theory Appl.*, vol. 46, no. 11, pp. 2038–2052, 2018.

[57] B. K. Bose, "Power electronics and motor drives recent progress and perspective," *IEEE Trans. Ind. Electron.*, vol. 56, no. 2, pp. 581–588, 2008.

[58] G. M. Sriramagiri, W. Luc, F. Jiao, K. Ayers, K. D. Dobson, and S. S. Hegedus, "Computation and assessment of solar electrolyzer field performance: Comparing coupling strategies," *Sustain. Energy Fuels*, vol. 3, no. 2, pp. 422–430, 2019.

[59] *Evaluation of measurement data—Guide to the expression of uncertainty in measurement*, International Organization for Standardization, JCGM, vol. 50. 2008.